

1 **Historical (1700–2012) Global Multi-model Estimates of the Fire Emissions from**  
2 **the Fire Modeling Intercomparison Project (FireMIP)**

3 Fang Li<sup>1\*</sup>, Maria Val Martin<sup>2</sup>, Meinrat O. Andreae<sup>3,4</sup>, Almut Arneth<sup>5</sup>, Stijn Hantson<sup>6,5</sup>,  
4 Johannes W. Kaiser<sup>7,3</sup>, Gitta Lasslop<sup>8</sup>, Chao Yue<sup>9,10</sup>, Dominique Bachelet<sup>11</sup>, Matthew  
5 Forrest<sup>8</sup>, Erik Kluzek<sup>12</sup>, Xiaohong Liu<sup>13</sup>, Stephane Mangeon<sup>14,15</sup>, Joe R. Melton<sup>16</sup>,  
6 Daniel S. Ward<sup>17</sup>, Anton Darmenov<sup>18</sup>, Thomas Hickler<sup>8,19</sup>, Charles Ichoku<sup>20</sup>, Brian I.  
7 Magi<sup>21</sup>, Stephen Sitch<sup>22</sup>, Guido R. van der Werf<sup>23</sup>, Christine Wiedinmyer<sup>24</sup>, Sam S.  
8 Rabin<sup>5</sup>

9  
10 <sup>1</sup> International Center for Climate and Environment Sciences, Institute of Atmospheric  
11 Physics, Chinese Academy of Sciences, Beijing, China

12 <sup>2</sup> Leverhulme Center for Climate Change Mitigation, Department of Animal & Plant  
13 Sciences, Sheffield University, Sheffield, UK

14 <sup>3</sup> Max Planck Institute for Chemistry, Mainz, Germany

15 <sup>4</sup> Department of Geology and Geophysics, King Saud University, Riyadh, Saudi Arabia

16 <sup>5</sup> Karlsruhe Institute of Technology (KIT), Institute of Meteorology and Climate  
17 research, Atmospheric Environmental Research, Garmisch-Partenkirchen, Germany

18 <sup>6</sup> Geospatial Data Solutions Center, University of California, Irvine, CA, USA

19 <sup>7</sup> Deutscher Wetterdienst, Offenbach, Germany

20 <sup>8</sup> Senckenberg Biodiversity and Climate Research Institute (BiK-F),

21 Senckenberganlage, Germany<sup>9</sup> State Key Laboratory of Soil Erosion and Dryland

22 Farming on the Loess Plateau, Northwest A&F University, Yangling, Shanxi, China

23 <sup>10</sup> Laboratoire des Sciences du Climat et de l'Environnement, LSCE/IPSL,  
24 CEA-CNRS-UVSQ, Université Paris-Saclay, Gif-sur-Yvette, France

25 <sup>11</sup> Biological and Ecological Engineering, Oregon State University, Corvallis, OR,  
26 USA

27 <sup>12</sup> National Center for Atmospheric Research, Boulder, CO, USA

28 <sup>13</sup> Department of Atmospheric Science, University of Wyoming, Laramie, WY, USA

29 <sup>14</sup> Department of Physics, Imperial College London, London, UK

30 <sup>15</sup> Now at CSIRO, Data61, Brisbane, QLD, Australia

31 <sup>16</sup> Climate Research Division, Environment and Climate Change Canada, Victoria, BC,  
32 Canada

33 <sup>17</sup> Karen Clark and Company, Boston, MA, USA

34 <sup>18</sup> Global Modeling and Assimilation Office, NASA Goddard Space Flight Center,  
35 Greenbelt, MD, USA

36 <sup>19</sup> Department of Physical Geography, Goethe University, Frankfurt am Main,  
37 Germany

38 <sup>20</sup> Howard University, NW, Washington, DC, USA

39 <sup>21</sup> Department of Geography and Earth Sciences, University of North Carolina at  
40 Charlotte, Charlotte, NC, USA

41 <sup>22</sup> College of Life and Environmental Sciences, University of Exeter, Exeter, UK

42 <sup>23</sup> Faculty of Science, Vrije Universiteit, Amsterdam, The Netherlands

43 <sup>24</sup> University of Colorado Boulder, Boulder, CO, USA

44 \*Correspondence to: Fang Li ([lifang@mail.iap.ac.cn](mailto:lifang@mail.iap.ac.cn))

45 **Abstract**

46 Fire emissions are a critical component of carbon and nutrient cycles and strongly  
47 affect climate and air quality. Dynamic Global Vegetation Models (DGVMs) with  
48 interactive fire modeling provide important estimates for long-term and large-scale  
49 changes in fire emissions. Here we present the first multi-model estimates of global  
50 gridded historical fire emissions for 1700–2012, including carbon and 33 species of  
51 trace gases and aerosols. The dataset is based on simulations of nine DGVMs with  
52 different state-of-the-art global fire models that participated in the Fire Modeling  
53 Intercomparison Project (FireMIP), using the same and standardized protocols and  
54 forcing data, and the most up-to-date fire emission factor table based on field and  
55 laboratory studies in various land cover types. We evaluate the simulations of  
56 present-day fire emissions by comparing them with satellite-based products. The  
57 evaluation results show that most DGVMs simulate present-day global fire emission  
58 totals within the range of satellite-based products. They can capture the high emissions  
59 over the tropical savannas and low emissions over the arid and sparsely vegetated  
60 regions, and the main features of seasonality. However, most models fail to simulate  
61 the interannual variability, partly due to a lack of modeling peat fires and tropical  
62 deforestation fires. Before the 1850s, all models show only a weak trend in global fire  
63 emissions, which is consistent with the multi-source merged historical reconstructions  
64 used as input data for CMIP6. On the other hand, the trends are quite different among  
65 DGVMs for the 20th century, with some models showing an increase and others a  
66 decrease in fire emissions, mainly as a result of the discrepancy in their simulated

67 responses to human population density change and land-use and land-cover change  
68 (LULCC). Our study provides an important dataset for further development of regional  
69 and global multi-source merged historical reconstructions, analyses of the historical  
70 changes in fire emissions and their uncertainties, and quantification of the role of fire  
71 emissions in the Earth system. It also highlights the importance of accurately modeling  
72 the responses of fire emissions to LULCC and population density change in reducing  
73 uncertainties in historical reconstructions of fire emissions and providing more reliable  
74 future projections.

75

## 76 **1. Introduction**

77 Fire is an intrinsic feature of terrestrial ecosystem ecology, occurring in all major  
78 biomes of the world soon after the appearance of terrestrial plants over 400 million  
79 years ago (Scott and Glasspool, 2006; Bowman et al., 2009). Fire emissions affect the  
80 Earth system in several important ways. First, chemical species emitted from fires are  
81 a key component of the global and regional carbon budgets (Bond-Lamberty et al.,  
82 2007; Ciais et al., 2013; Kondo et al., 2018), a major source of greenhouse gases (Tian  
83 et al., 2016), and the largest contributor of primary carbonaceous aerosols globally  
84 (Andreae and Rosenfeld, 2008; Jiang et al., 2016). Second, by changing the  
85 atmospheric composition, fire emissions affect the global and regional radiation  
86 balance and climate (Ward et al., 2012; Tosca et al. 2013; Jiang et al., 2016; Grandey et  
87 al., 2016; McKendry et al., 2019; Hamilton et al., 2018; Thornhill et al., 2018). Third,  
88 fire emissions change the terrestrial nutrient and carbon cycles through altering the

89 deposition of nutrients (e.g., nitrogen, phosphorus), surface ozone concentration, and  
90 meteorological conditions (Mahowald et al., 2008; Chen et al., 2010; McKendry et al.,  
91 2019; Yue and Unger, 2018). In addition, they degrade the air quality (Val Martin et al.,  
92 2015; Knorr et al., 2017), which poses a significant risk to human health and has been  
93 estimated to result in at least ~165,000, and more likely ~339,000 pre-mature deaths per  
94 year globally (Johnston et al., 2012; Marlier et al., 2013; Lelieveld et al., 2015).

95 To date, only emissions from individual fires or small-scale fire complexes can be  
96 directly measured from field campaigns and laboratory experiments (Andreae and  
97 Merlet, 2001; Yokelson et al., 2013; Stockwell et al., 2016; Andreae, 2019).  
98 Regionally and globally, fire emissions are often estimated based on satellite  
99 observations, fire proxy records, and numerical models, even though some attempts  
100 have been made to bridge the gap between local observations and regional estimations  
101 using combinations of aircraft and ground based measurements from field campaigns  
102 (e.g., SAMBBA, ARCTAS), satellite-based inventories, and chemical transport  
103 models (e.g., Fisher et al., 2010; Reddington et al., 2019; Konovalov et al., 2018).  
104 Satellite-based fire emission estimates are primarily derived from satellite observations  
105 of burned area, active fire counts, and/or fire radiative power, and are sometimes  
106 constrained by satellite observations of aerosol optical depth (AOD), CO, or CO<sub>2</sub>  
107 (Wiedinmyer et al., 2011; Kaiser et al., 2012; Krol et al., 2013; Konovalov et al., 2014;  
108 Ichoku and Ellison, 2014; Darmenov and da Silva, 2015; van der Werf et al., 2017;  
109 Heymann et al., 2017). Satellite-based fire emission estimates are available globally,

110 but cover only the present-day period, i.e., since 1997 for Global Fire Emissions  
111 Dataset (GFED) and shorter periods for others.

112 Historical change of fire emissions has been inferred from a variety of proxies,  
113 such as ice-core records of CH<sub>4</sub> (isotope  $\delta^{13}\text{C}$  from pyrogenic or biomass burning  
114 source), black carbon, levoglucosan, vanillic acid, ammonium, and CO (Ferretti et al.,  
115 2005; McCormell et al., 2007; Conedera et al., 2009; Wang et al., 2012; Zennaro et al.,  
116 2014), site-level sedimentary charcoal records (Marlon et al., 2008, 2016), visibility  
117 records (van Marle et al., 2017a), and fire-scar records (Falk et al. 2011). Fire proxies  
118 can be used to reconstruct fire emissions on a local to global scale and for time  
119 periods of decades to millennia and beyond. However, they are of limited spatial extent  
120 and cannot be directly converted into emission amounts. Moreover, large uncertainties  
121 and discrepancies were shown in their inferred regional or global long-term trends due  
122 to limited sample size and often unclear representative areas and time periods of fire  
123 emissions (Pechony and Shindell, 2010; van der Werf et al., 2013; Legrand et al.,  
124 2016).

125 Dynamic Global Vegetation Models (DGVMs) that include fire modeling are  
126 indispensable for estimating fire carbon emissions at local to global scales for past,  
127 present, and future periods (Hantson et al., 2016). These models represent interactions  
128 among fire dynamics, biogeochemistry, biogeophysics, and vegetation dynamics at the  
129 land surface within a physically and chemically consistent modeling framework.

130 DGVMs are often used as the terrestrial ecosystem component of Earth System models  
131 (ESMs) and have been widely applied in global change research (Levis et al., 2004; Li

132 et al., 2013; Kloster and Lasslop, 2017). Fire emissions of trace gases and aerosols can  
133 be derived from the product of fire carbon emissions simulated by DGVMs and fire  
134 emission factors (Li et al., 2012; Knorr et al., 2016).

135 Modeling fire and fire emissions within DGVMs started in the early 2000s  
136 (Thonicke et al., 2001), and has rapidly progressed during the past decade (Hantson et  
137 al., 2016). The Fire Model Intercomparison Project (FireMIP) initiated in 2014 was the  
138 first international collaborative effort to better understand the behavior of global fire  
139 models (Hantson et al., 2016). A set of common fire modeling experiments driven by  
140 the same forcing data were performed (Rabin et al., 2017). Nine DGVMs with different  
141 state-of-the-art global fire models participated in FireMIP. All global fire models used  
142 in the upcoming 6<sup>th</sup> Coupled Model Intercomparison Project (CMIP6) and IPCC AR6  
143 are included in FireMIP, except for the fire scheme in GFDL-ESM (Rabin et al., 2018;  
144 Ward et al., 2018) which is similar to that of CLM4.5 (Li et al., 2012) in FireMIP. Note  
145 that GlobFIRM (Thonicke et al., 2001) in FireMIP is the most commonly-used fire  
146 scheme in CMIP5 (Kloster and Lasslop, 2017), and is still used by some models in  
147 CMIP6.

148 Earlier studies provided only one single time series of fire emissions for global  
149 grids or regions (Schultz et al., 2008; Mieville et al., 2010; Lamarque et al., 2010;  
150 Marlon et al., 2016; van Marle et al., 2017b; and references therein). This limits their  
151 utility for quantifying the uncertainties in global and regional reconstructions of fire  
152 emissions and the corresponding impacts on estimated historical changes in carbon  
153 cycle, climate, and air pollution. A small number of studies also investigated the

154 drivers of fire carbon emission trends (Kloster et al., 2010; Yang et al., 2014; Li et al.,  
155 2018; Ward et al., 2018). However, these studies could not identify the uncertainty  
156 source in recent model-based reconstructions or help understand the inter-model  
157 discrepancy in projections of future fire emissions because only a single DGVM was  
158 used in each.

159 This study provides a new dataset of global gridded fire emissions, including  
160 carbon and 33 species of trace gases and aerosols, over the 1700–2012 time period,  
161 based on nine DGVMs with different state-of-the-art global fire models that  
162 participated in FireMIP. The dataset provides a basis for developing multi-source (e.g.,  
163 satellite-based products, model simulations, and/or fire proxy records) merged fire  
164 emission reconstructions and methods. It also, for the first time, allows end users to  
165 select all or a subset of model-based reconstructions that best suits their regional or  
166 global research needs. Importantly, it enables the quantification of the uncertainty  
167 range of past fire emissions and their impacts. In addition, the model-based estimates  
168 of fire emissions are comprehensively evaluated through comparison with  
169 satellite-based products, including amounts, spatial distribution, seasonality, and  
170 interannual variability, thus providing information on the limitations of recent  
171 model-based reconstructions. We also analyze the simulated long-term changes and  
172 the drivers for each DGVM and inter-model differences.

173

## 174 **2 Methods and datasets**

### 175 **2.1 Models in FireMIP**



176 Nine DGVMs with different fire modules participated in FireMIP: CLM4.5 with CLM5  
177 fire module, CTEM, JSBACH-SPITFIRE, JULES-INFERNO,  
178 LPJ-GUESS-GlobFIRM, LPJ-GUESS-SIMFIRE-BLAZE, LPJ-GUESS-SPITFIRE,  
179 MC2, and ORCHIDEE-SPITFIRE (Table 1, see Rabin et al., 2017 for detailed  
180 description of each model). JSBACH, ORCHIDEE, and LPJ-GUESS used the variants  
181 of SPITFIRE (Thonicke et al., 2010) with updated representation of human ignition  
182 and suppression, fuel moisture, combustion completeness, and the relationship  
183 between spread rate and wind speed for JSBACH (Lasslop et al., 2014), combustion  
184 completeness for ORCHIDEE (Yue et al., 2014, 2015), and human ignition, post-fire  
185 mortality factors, and modifications for matching tree age/size structure for  
186 LPJ-GUESS (Lehsten et al., 2009; Rabin et al., 2017).

187 The global fire models in the nine DGVMs have diverse levels of complexity  
188 (Rabin et al., 2017). SIMFIRE is a statistical model based on present-day  
189 satellite-based fire products (Knorr et al., 2016). In CLM4.5, crop, peat, and tropical  
190 deforestation fires are empirically/statistically modeled (Li et al., 2013). The scheme  
191 for fires outside the tropical closed forests and croplands in CLM4.5 (Li et al., 2012;  
192 Li and Lawrence, 2017), fire modules in CTEM (Arora and Boer, 2005; Melton and  
193 Arora, 2016), GlobFIRM (Thonicke, 2001), and INFERNO (Mangeon et al., 2016) are  
194 process-based and of intermediate-complexity. That is, area burned is determined by  
195 two processes: fire occurrence and fire spread, but with simple empirical/statistical  
196 equations for each process. Fire modules in MC2 (Bachelet et al., 2015; Sheehan et al.,  
197 2015) and SPITFIRE variants are more complex, which use the Rothermel equations

198 (Rothermel, 1972) to model fire spread and consider the impact of fuel composition on  
199 fire behavior.

200 How humans affect fires differs among these global fire models (Table 2), which  
201 influences their estimates of fire emissions. GlobFIRM does not consider any direct  
202 human effect on fires and MC2 fire model only considers human suppression on fire.  
203 CLM4.5 models fires in croplands, human deforestation and degradation fires in  
204 tropical closed forests, and human ignition and suppression for both occurrence and  
205 spread of fires outside of tropical closed forests and croplands. Burned area in  
206 SIMFIRE and human influence on fire occurrence in other models are a non-linear  
207 function of population density. CTEM and JSBACH-SPITFIRE also consider human  
208 suppression on fire duration. JULES-INFERNO treats croplands and crop fires as  
209 natural grasslands and grassland fires. All models, except for CLM4.5 and INFERNO,  
210 set burned area to zero in croplands. FireMIP models treat pasture fires as natural  
211 grassland fires by using the same parameter values if they have pasture plant functional  
212 types (PFTs) or lumping pastures with natural grasslands otherwise. Biomass harvest is  
213 considered in pastures in LPJ-GUESS-GlobFIRM and LPJ-GUESS-SIMFIRE-BLAZE,  
214 which decreases fuel availability for fires, and that JSBACH-SPITFIRE sets high fuel  
215 bulk density for pasture PFTs.

216 Only CLM4.5 simulates peat fires, although only emissions from burning of  
217 vegetation tissues and litter are included in outputs for FireMIP, i.e., burning of soil  
218 organic matter is not included (Table 2).

219 In the FireMIP models, fire carbon emissions are calculated as the product of  
220 burned area, fuel load, and combustion completeness. Combustion completeness is the  
221 fraction of live plant tissues and ground litter burned (0–100%). It depends on PFT and  
222 plant tissue type in GlobFIRM and in the fire modules of CLM4.5 and CTEM, and is  
223 also a function of soil moisture in INFERNO. Combustion completeness depends on  
224 plant tissue type and surface fire intensity in SIMFIRE, fuel type and wetness in the  
225 SPITFIRE family models, and fuel type, load, and moisture in MC2 fire module.

226

## 227 **2.2 FireMIP experimental protocol and input datasets**

228 The nine DGVMs in FireMIP are driven with the same forcing data (Rabin et al.,  
229 2017). The atmospheric forcing is from CRU-NCEP v5.3.2 with a spatial resolution of  
230  $0.5^\circ$  and a 6-hourly temporal resolution (Wei et al., 2014). The 1750–2012 annual  
231 global atmospheric  $\text{CO}_2$  concentration is derived from ice core and NOAA monitoring  
232 station data (Le Quéré et al., 2014). Annual land-use and land-cover change (LULCC)  
233 and population density at a  $0.5^\circ$  resolution for 1700–2012 are from Hurtt et al. (2011)  
234 and Klein Goldewijk et al. (2010, HYDE v3.1), respectively. Monthly cloud-to-ground  
235 lightning frequency for 1901–2012, at  $0.5^\circ$  resolution, is derived from the observed  
236 relationship between present-day lightning and convective available potential energy  
237 (CAPE) anomalies (Pfeiffer et al., 2013, J. Kaplan, personal communication,  
238 2015). Fire emissions in this study are estimated using the model outputs of PFT-level  
239 fire carbon emissions and vegetation characteristics (PFTs and their fractional area  
240 coverages) from the FireMIP historical transient control run (SF1) (Rabin et al., 2017).

241 SF1 includes three phases (Fig. 1): the 1700 spin-up phase, the 1701–1900 transient  
242 phase, and the 1901–2012 transient phase. In the 1700 spin-up phase, all models are  
243 spun up to equilibrium, forced by population density and prescribed LULCC at their  
244 1700 values, 1750 atmospheric CO<sub>2</sub> concentration, and the repeatedly cycled 1901–  
245 1920 atmospheric forcing (precipitation, temperature, specific humidity, surface  
246 pressure, wind speed, and solar radiation) and lightning data. The 1701–1900 transient  
247 phase is forced by 1701–1900 time-varying population and LULCC, with constant CO<sub>2</sub>  
248 concentration at 1750 level until 1750 and time-varying CO<sub>2</sub> concentration for 1750–  
249 1900, and the cycled 1901–1920 atmospheric forcing and lightning data. In the 1901–  
250 2012 transient phase, models are driven by 1901–2012 time-varying population density,  
251 LULCC, CO<sub>2</sub> concentration, atmospheric forcing, and lightning data. Unlike all other  
252 models, MC2 and CTEM run from 1901 and 1861, respectively, rather than 1700.

253 Six FireMIP models (CLM4.5, JSBACH-SPITFIRE, JULES-INFERNO,  
254 LPJ-GUESS-SPITFIRE, LPJ-GUESS-SIMFIRE-BLAZE, and  
255 ORCHIDEE-SPITFIRE) also provide outputs of five sensitivity simulations: constant  
256 climate, constant atmospheric CO<sub>2</sub> concentration, constant land cover, constant  
257 population density, and constant lightning frequency throughout the whole simulation  
258 period. The sensitivity simulations are helpful for understanding the drivers of changes  
259 in reconstructed fire emissions.

260

### 261 **2.3 Estimates of fire trace gas and aerosol emissions**

262 Based on fire carbon emissions and vegetation characteristics from DGVMs and fire  
263 emission factors, fire emissions of trace gas and aerosol species  $i$  and the PFT  $j$ ,  $E_{ij}$  (g  
264 species  $\text{m}^{-2} \text{s}^{-1}$ ), are estimated according to Andreae and Merlet (2001):

$$265 \quad E_{ij} = EF_{ij} \times CE_j / [C], \quad (1)$$

266 where  $EF_{ij}$  (g species (kg dry matter (DM))<sup>-1</sup>) is a PFT-specific emission factor (EF),  
267  $CE_j$  denotes the fire carbon emissions of PFT  $j$  (g C  $\text{m}^{-2} \text{s}^{-1}$ ), and  $[C]=0.5 \times 10^3$  g C (kg  
268 DM)<sup>-1</sup> is a unit conversion factor from carbon to dry matter.

269 The EFs used in this study (Table 3) are based on Andreae and Merlet (2001), with  
270 updates from field and laboratory studies over various land cover types published  
271 during 2001–2018 (Andreae, 2019). All FireMIP model simulations used the same  
272 EFs from Table 3.

273 DGVMs generally simulate vegetation as mixture of PFTs in a given grid  
274 location to represent plant function at global scale, instead of land cover types. In  
275 Table 4, we associate the PFTs from each DGVM to the land cover types shown in  
276 Table 3. Grass, shrub, savannas, woodland, pasture, tundra PFTs are classified as  
277 grassland/savannas. Tree PFTs and crop PFTs are classified as forests and croplands,  
278 respectively, similar to Li et al. (2012), Mangeon et al. (2016), and Melton and Arora  
279 (2016). PFTs of evergreen tree and other broadleaf deciduous tree in CTEM,  
280 extra-tropical evergreen and deciduous tree in JSBACH, and broadleaf deciduous tree  
281 and needleleaf evergreen tree in JULES are divided into tropical, temperate, and boreal  
282 groups following Nemani and Running (1996).

283 We provide two versions of fire emission products with different spatial  
284 resolutions: the original spatial resolution for each FireMIP DGVM outputs (Table 1),  
285 and a 1x1 degree horizontal resolution. For the latter, fire emissions are unified to 1  
286 degree resolution using bilinear interpolation for CLM4.5, CTEM, JSBACH, and  
287 JULES which have coarser resolution, and area-weighted averaging-up for other  
288 models whose original resolution is 0.5 degree. The 1x1 degree product is used for  
289 present-day evaluation and historical trend analyses in Sects. 3 and 4.

290

## 291 **2.4 Benchmarks**

292 Satellite-based products are commonly used as benchmarks to evaluate present-day  
293 fire emission simulations (Rabin et al., 2017, and references therein). In the present  
294 study, six satellite-based products are used (Table 5). Fire emissions in  
295 GFED4/GFED4s (small fires included in GFED4s) (van der Werf et al., 2017),  
296 GFAS1.2 (Kaiser et al., 2012), and FINN1.5 (Wiedinmyer et al., 2011) are based on  
297 emission factor (EF) and fire carbon emissions (CE) (Eq. 1). CE is estimated from  
298 MODIS burned area and VIRS/ATSR active fire products in the GFED family,  
299 MODIS active fire detection in FINN1.5, and MODIS fire radiative power (FRP) in  
300 GFAS1. Fire emissions from FEER1 (Ichoku and Ellison, 2014) and QFEDv2.5  
301 (Darmenov and da Silva, 2015) are derived using FRP, and constrained with satellite  
302 AOD observations. Satellite-based present-day fire emissions for the same region can  
303 differ by a factor of 2–4 on an annual basis (van der Werf et al., 2010) and up to 12 on a  
304 monthly basis (Zhang et al., 2014). The discrepancy among satellite-based estimates of

305 present-day fire emissions mainly comes from the satellite observations used, the  
306 methods applied for deriving fire emissions, and the emissions factors.

307

## 308 **2.5 Multi-source merged historical reconstructions**

309 We also compared the simulated historical changes with historical reconstructions  
310 merged from multiple sources used as forcing data for CMIPs. Fire emission estimates  
311 for CMIP5 and CMIP6 were merged from different sources (Table 5). For CMIP5  
312 (Lamarque et al., 2010), the decadal fire emissions are available from 1850 to 2000,  
313 estimated using GFED2 fire emissions (van der Werf et al., 2006) for 1997 onwards,  
314 RETRO (Schultz et al., 2008) for 1960–1900, GICC (Mieville et al., 2010) for  
315 1900–1950, and kept constant at the 1900 level for 1850–1900. RETRO combined  
316 literature reviews with satellite-based fire products and the GlobFIRM fire model.  
317 GICC is based on a burned area reconstruction from literature review and sparse tree  
318 ring records (Mouillot et al., 2005), satellite-based fire counts, land cover map, and  
319 representative biomass density and burning efficiency of each land cover type.

320 For CMIP6, monthly fire emission estimates are available from 1750 to 2015 (van  
321 Marle et al., 2017b). The CMIP6 estimates are merged from GFED4s fire carbon  
322 emissions for 1997 onwards, charcoal records GCDv3 (Marlon et al., 2016) for North  
323 America and Europe, visibility records for Equatorial Asia (Field et al., 2009) and  
324 central Amazon (van Marle et al., 2017b), and the median of simulations of six  
325 FireMIP models (CLM4.5, JSBACH-SPITFIRE, JULES-INFERNO,  
326 LPJ-GUESS-SPITFIRE, LPJ-GUESS-SIMFIRE-BLAZE, and

327 ORCHIDEE-SPITFIRE) for all other regions. Then, based on the merged fire carbon  
328 emissions, CMIP6 fire trace gas and aerosol emissions are derived using EF from  
329 Andreae and Merlet (2001) with updates to 2013 and Akagi et al. (2011) with updates  
330 for temperate forests to 2014, and a present-day land cover map.

331

### 332 **3 Evaluation of present-day fire emissions**

333 The spatial pattern and temporal variability of different fire emission species are  
334 similar, with some slight differences resulting from the estimated fire carbon emissions  
335 from the land cover types that have different emission factors (Table 3). Therefore, we  
336 focus on several important species as examples to exhibit the performance of FireMIP  
337 models on the simulations of present-day fire emissions.

338

#### 339 **3.1 Global amounts and spatial distributions**

340 As shown in Table 6, FireMIP models, except for MC2 and LPJ-GUESS-GlobFIRM,  
341 estimate present-day fire carbon, CO<sub>2</sub>, CO, CH<sub>4</sub>, BC, OC, and PM<sub>2.5</sub> annual emissions  
342 to be within the range of satellite-based products. For example, the estimated range of  
343 fire carbon emissions is 1.7–3.0 Pg C yr<sup>-1</sup>, whereas it is 1.5–4.2 Pg C yr<sup>-1</sup> for  
344 satellite-based products. Low fire emissions in MC2 result from relatively low  
345 simulated global burned area, only about 1/4 of satellite-based observations (Andela et  
346 al., 2017). In contrast, high emissions in LPJ-GUESS-GlobFIRM are mainly due to the  
347 higher combustion completeness of woody tissues (70–90% of stem and coarse woody  
348 debris burned in post-fire regions) than those used in other FireMIP models (Table 2)



349 and the satellite-based GFED family (20–40% for stem and 40–60% for coarse woody  
350 debris) (van der Werf et al., 2017).

351 FireMIP DGVMs, except for MC2, represent the general spatial distribution of  
352 fire emissions evident in satellite-based products, with high fire BC emissions over  
353 tropical savannas and low emissions over the arid and sparsely vegetated regions (Fig.  
354 2). Among the nine models, CLM4.5, JULES-INFERNO, and  
355 LPJ-GUESS-SIMFIRE-BLAZE have higher global spatial pattern correlation with  
356 satellite-based products than the other models, indicating higher skill in their  
357 spatial-pattern simulations. It should also be noted that, on a regional scale, CTEM,  
358 JULES-INFERNO, LPJ-GUESS-SPITFIRE, and ORCHIDEE-SPITFIRE  
359 underestimate fire emissions over boreal forests in Asia and North America.  
360 LPJ-GUESS-GlobFIRM and LPJ-GUESS-SIMFIRE-BLAZE overestimate fire  
361 emissions over the Amazon and African rainforests. CLM4.5 and  
362 LPJ-GUESS-GlobFIRM overestimate fire emissions over eastern China.  
363 JSBACH-SPITFIRE underestimates fire emissions in most tropical forests. MC2  
364 underestimates fire emissions over most regions, partly because it allows only one  
365 ignition per year per grid cell and thus underestimates the burned area.

366 We further analyze the spatial distribution of inter-model differences. As shown in  
367 Fig. 3, the main disagreement among FireMIP models occurs in the tropics, especially  
368 over the tropical savannas in Africa, South America, and northern Australia. This is  
369 mainly driven by the MC2, CTEM, JSBACH-SPITFIRE, and ORCHIDEE-SPITFIRE  
370 simulations (Fig. 2). Differences among the satellite-based estimates have a similar

371 spatial pattern, but higher than the inter-model spread in savannas over southern  
372 Africa and lower in the temperate arid and semi-arid regions and north of 60°N over  
373 Eurasia (Fig. S1a).

374

### 375 **3.2 Seasonal cycle**

376 The FireMIP models reproduce similar seasonality features of fire emissions to  
377 satellite-based products, that is, peak month is varied from the dry season in the tropics  
378 to the warm season in the extra-tropics (Fig. 4).

379 For the tropics in the Southern Hemisphere, fire PM<sub>2.5</sub> emissions of  
380 satellite-based products peak in August–September. Most FireMIP models can  
381 reproduce this pattern, except ORCHIDEE-SPITFIRE and LPJ-GUESS-SPITFIRE  
382 peaking two months and one month earlier, respectively, and JSBACH-SPITFIRE with  
383 much lower amplitude of seasonal variability likely caused by parameter setting in its  
384 fuel moisture functions (Table S9 in Rabin et al. (2017)).

385 For the tropics in the Northern Hemisphere, most FireMIP models exhibit larger  
386 fire emissions in the northern winter, consistent with the satellite-based products.

387 In the northern extra-tropical regions, satellite-based products show two periods  
388 of high values: April–May resulting mainly from fires in croplands and grasslands, and  
389 July mainly due to fires in the boreal evergreen forests. Most FireMIP models can  
390 reproduce the second one, except for LPJ-GUESS-SPITFIRE which peaks in October.  
391 CLM4.5 is the only model that can capture both peak periods partly because it's the  
392 only one to consider unique seasonality of crop fires.

393

### 394 **3.3 Interannual variability**

395 Global fire PM<sub>2.5</sub> emissions from satellite-based products for 1997–2012 show a  
396 substantial interannual variability, which peaks in 1997–1998, followed by a low  
397 around 2000 and a decline starting in 2002–2003 (Fig. 5). The 1997–1998 high  
398 emission values are caused by peat fires in Equatorial Asia in 1997 and widespread  
399 drought-induced fires in 1998 associated with the most powerful El Niño event in  
400 1997–1998 recorded in history (van der Werf et al., 2017; Kondo et al., 2018). Most  
401 FireMIP models cannot reproduce the 1997–1998 peak, except for CLM4.5 as the  
402 only model that simulates the burning of plant-tissue and litter from peat fires  
403 (although burning of soil organic matter is not included) and the drought-linked  
404 tropical deforestation and degradation fires (Li et al., 2013, Kondo et al., 2018).  
405 CLM4.5, CTEM, and LPJ-GUESS-SIMFIRE-BLAZE present the highest temporal  
406 correlation between models and satellite-based products (0.55–0.79 for CLM4.5, 0.51–  
407 0.68 for CTEM, and 0.39–0.72 for LPJ-GUESS-SIMFIRE-BLAZE), and thus are  
408 more skillful than other models to reproduce the interannual variability observed from  
409 satellite-based products (Table 7).

410 We use the coefficient of variation (CV, the standard deviation divided by the  
411 mean, %) to represent the amplitude of interannual variability of fire emissions. As  
412 shown in Fig. 5, for 1997–2012, all FireMIP models underestimate the variation as a  
413 result of (at least) partially missing the 1997–1998 fire emission peak. For 2003–2012  
414 (the common period of all satellite-based products and models), interannual variation

415 of annual fire PM<sub>2.5</sub> emissions in CLM4.5, CTEM, and LPJ-GUESS family models lies  
416 within the range of satellite-based products (CV=6–12%). Other models present  
417 weaker variation (CV=5%) except for MC2 (CV=24%) that has a much stronger  
418 variation than all satellite-based products and other FireMIP models.

419

## 420 **4 Historical changes and drivers**

### 421 **4.1 Historical changes**

422 Figure 6 shows historical simulations of the FireMIP models as well as the CMIP5 and  
423 CMIP6 reconstructions for fire carbon, CO<sub>2</sub>, CO, and PM<sub>2.5</sub> emissions. We find similar  
424 historical changes for all the species, with the maximum global fire emissions given by  
425 LPJ-GUESS-GlobFIRM and the minima by LPJ-GUESS-SPITFIRE before 1901 and  
426 MC2 afterwards.

427 Long-term trends in simulated global fire emissions for all models are weak  
428 before the 1850s (relative trend <0.015% yr<sup>-1</sup>). They are similar to CMIP6 estimates  
429 (Fig. 6), but in disagreement with earlier reconstructions based on charcoal records  
430 (Marlon et al., 2008; Marlon et al., 2016), ice-core CO records (Wang et al., 2010),  
431 and ice-core δ<sup>13</sup>CH<sub>4</sub> records (Ferretti et al., 2005), which exhibit a rapid increase from  
432 1700 to roughly the 1850s. After the 1850s, disagreement in the trends among FireMIP  
433 models begins to emerge. Fire emissions in LPJ-GUESS-SIMFIRE-BLAZE decline  
434 since ~1850, while fire emissions in LPJ-GUESS-SPITFIRE, MC2, and  
435 ORCHIDEE-SPITFIRE show upward trends from ~1900s. In CLM4.5, CTEM, and  
436 JULES-INFERNO, fire emissions increase slightly before ~1950, similar to the

437 CMIP6 estimates, but CTEM and JULES-INFERNO decrease thereafter, contrary to  
438 CMIP5 and CMIP6 estimates and CLM4.5. JSBACH-SPITFIRE simulates a decrease  
439 of fire emissions before 1940s and an increase later, similar to the CMIP5 estimates.  
440 All the long-term trends described above are significant at the 0.05 level using the  
441 Mann-Kendall trend test.

442 Earlier reconstructions based on fire proxies also show a big difference in  
443 long-term changes after the 1850s. The reconstruction based on the Global Charcoal  
444 Database version 3 (GCDv3, Marlon et al., 2016) exhibits a decline from the late 19th  
445 century to the 1920s, and then an upward trend until ~1970, followed by a drop. The  
446 reconstructions based on the GCDv1 (Marlon et al., 2008) and ice-core CO records  
447 (Wang et al., 2010) show a sharp drop since roughly the 1850s, while a steady rise is  
448 exhibited in the reconstruction based on ice-core  $\delta^{13}\text{CH}_4$  records (Ferretti et al., 2005).  
449 The simulated historical changes of FireMIP models (Fig. 6) fall into this fairly broad  
450 range of long-term trends in these reconstructions.

451 Spatial patterns of inter-model spread of fire emissions for 1700–1850 and 1900–  
452 2000 (Figs. S1b–c) are similar to the present-day patterns as shown in Fig. 3.

453

#### 454 **4.2 Drivers**

455 Six FireMIP models also conducted sensitivity experiments, which can be used to  
456 isolate the role of individual forcing factors in long-term trends of fire emissions  
457 during the 20th century. The median of the six models are also used for building  
458 CMIP6 fire emission estimates (van Marle et al. 2017b). The 20th century changes of

459 driving forces used in FireMIP are characterized by an increase in the global land  
460 temperature, precipitation, lightning frequency, atmospheric CO<sub>2</sub> concentration,  
461 population density, cropland and pasture areas, and a decrease in the global forest area  
462 (Teckentrup et al., 2019).

463 As shown in Figs. 6 and 7, the downward trend of global fire emissions in  
464 LPJ-GUESS-SIMFIRE-BLAZE is mainly caused by LULCC and increasing  
465 population density. Upward trends in LPJ-GUESS-SPITFIRE and  
466 ORCHIDEE-SPITFIRE are dominated by LULCC and rising population density and  
467 CO<sub>2</sub> during the 20th century. In CLM4.5 and JULES-INFERNO, upward trends before  
468 ~1950 are attributed to rising CO<sub>2</sub>, climate change, and LULCC, and the subsequent  
469 drop in JULES-INFERNO mainly results from the rising population density and  
470 climate change. Long-term changes of global fire emissions in JSBACH-SPITFIRE are  
471 mainly driven by LULCC and rising CO<sub>2</sub>.

472 As shown in Fig. 7, the inter-model spread in long-term trends mainly arises from  
473 the simulated anthropogenic influence (LULCC and population density change) on fire  
474 emissions, as the standard deviation in simulated responses to LULCC (0.27 Pg C yr<sup>-1</sup>)  
475 and population density (0.11 Pg C yr<sup>-1</sup>) is much larger than the other drivers.

476 LULCC decreases global fire emissions sharply in  
477 LPJ-GUESS-SIMFIRE-BLAZE during the 20th century, but increases global fire  
478 emissions for the other models except for JSBACH-SPITFIRE. The response to  
479 LULCC in LPJ-GUESS-SIMFIRE-BLAZE is because it assumes no fire in croplands  
480 and accounts for biomass harvest (thus reducing fuel availability) in pastures (Table

481 2), the area of which expanded over the 20th century. The LULCC-induced increase  
482 in fire emissions for ORCHIDEE-SPITFIRE, LPJ-GUESS-SPITFIRE, and  
483 JULES-INFERNO are partly caused by increased burned area due to the expansion of  
484 grasslands (pastures are lumped in natural grasslands in these models) where fuels are  
485 easier to burn than woody vegetation in the model setups (Rabin et al., 2017).  
486 CLM4.5 models crop fires and tropical deforestation and degradation fires. Crop fire  
487 emissions in CLM4.5 are estimated to increase during the 20th century due to  
488 expansion of croplands and increased fuel loads over time (Fig. S2). Emissions of  
489 tropical deforestation and degradation fires in CLM4.5 are increased before ~1950,  
490 responding to increased human deforestation rate in tropical closed forests based on  
491 prescribed land use and land cover changes (Li et al. 2018). In JSBACH-SPITFIRE,  
492 as croplands and pastures expand over time, the assumption of no fire over croplands  
493 tends to decrease fire emissions, while the setting of high fuel bulk density for  
494 pastures tends to increase fire emissions due to increased fuel combusted per burned  
495 area, which together partly result in the shifted sign of response to LULCC around the  
496 1940s.

497 Rising population density throughout the 20th century decreases fire emissions in  
498 CLM4.5 and LPJ-GUESS-SIMFIRE-BLAZE because they include human suppression  
499 on both fire occurrence and fire spread. Fire suppression increases with rising  
500 population density and is simulated explicitly in CLM4.5 and implicitly in  
501 LPJ-GUESS-SIMFIRE-BLAZE. On the contrary, rising population density increases  
502 fire emissions in LPJ-GUESS-SPITFIRE and ORCHIDEE-SPITFIRE because

503 observed human suppression on fire spread found in Li et al. (2013), Hantson et al.  
504 (2015), and Andela et al. (2017) is not taken into account in the two models. The  
505 response to population density change for the other models is small, reflecting the  
506 compensating effects of human ignition and human suppression on fire occurrence  
507 (strongest in JULES-INFERNNO in FireMIP models), and also human suppression on  
508 fire duration (JSBACH-SPITFIRE).

509 All models simulate increased fire emissions with increased atmospheric CO<sub>2</sub>  
510 concentration since elevated CO<sub>2</sub> increases the fuel load. Elevated CO<sub>2</sub> increases both  
511 the photosynthetic uptake of CO<sub>2</sub> (Mao et al., 2009) and plant water-use efficiency (i.e.,  
512 less water stress on plant growth and succession, Keenan et al., 2013), that is, CO<sub>2</sub>  
513 fertilization effect, which can stimulate carbon uptake and storage by the terrestrial  
514 biosphere. Such a CO<sub>2</sub>-driven increase of fuel load is consistent with a recent analysis  
515 of satellite-derived vegetation indices (Zhu et al., 2016). FireMIP models also agree  
516 that impacts of changes in lightning frequency on long-term trends of fire emissions are  
517 small. Moreover, most FireMIP models agree that climate change tends to increase fire  
518 carbon emissions during the first several decades and then falls, reflecting co-impacts  
519 of climate on both fuel load and fuel moisture.

520

### 521 **4.3 Regional long-term changes**

522 We divided the global map into 14 regions following the definition of the GFED  
523 family (Fig. 8a). As shown in Fig. 8b, inter-model discrepancy in long-term changes



524 are largest in Southern Hemisphere South America (SHSA), southern and northern  
525 Africa (NHAF and SHAF), and central Asia (CEAS).

526 Most FireMIP models reproduce the upward trends of fire CO emissions found  
527 also in the CMIP5 or CMIP6 estimates since 1950s in SHSA and till ~1950 in Africa  
528 (Figs. 9e, h, and i). Long-term trends in regional fire emissions in SHSA, Africa, and  
529 central Asia can broadly explain the upward trends in global fire emissions in  
530 LPJ-GUESS-SPITFIRE, MC2, and ORCHIDEE-SPITFIRE, the downward trends in  
531 LPJ-GUESS-SIMFIRE-BLAZE, and the rise followed by a drop in CTEM, whose  
532 global fire emissions exhibit most obvious long-term trends in FireMIP models (Fig.  
533 6).

534 In other regions, the difference in long-term changes among models is smaller (Fig.  
535 8b). Emissions of most models and CMIP5 estimates exhibit a significant decline in  
536 temperate North America (TENA) from ~1850 to ~1970, while historical changes of  
537 CMIP6 estimates are comparatively small (Fig. 9b). LPJ-GUESS-SIMFIRE-BLAZE  
538 has a more obvious long-term change than the other FireMIP models and CMIPs in  
539 boreal North America (BONA) and northern South America (NHSA) (Figs. 9a and d).  
540 MC2 and LPJ-GUESS-GlobFIRM emissions increase after ~1900 in Europe (EURO),  
541 while emissions of other models and CMIPs are overall constant (Fig. 9f). In boreal  
542 Asia (BOAS), emissions of most models and CMIP6 are relatively constant, while  
543 LPJ-GUESS-GlobFIRM and CMIP5 emissions decline from 1850 to the 1950s and  
544 from 1900 to the 1970s, respectively, and then rise (Fig. 9j). JULES,  
545 LPJ-GUESS-SIMFIRE-BLAZE, CLM4.5, CTEM, and CMIP6 emissions significantly

546 decline since the 1950s in Southeast Asia (SEAS), while CMIP5 emissions increase  
547 (Fig. 9l). In equatorial Asia (EQAS), CMIPs emissions increase after ~1950, which is  
548 partly reproduced by only CLM4.5 in FireMIP (Fig. 9m).

549 As shown in Figs. S3–5, long-term changes of regional fire emissions for other  
550 species are similar to those of fire CO emissions.

551 The long-term changes of regional fire emissions and inter-model disagreement  
552 are mainly caused by simulated responses to LULCC and/or population density change  
553 for the 20th century (Figs. S6–19). Besides, climate change also plays an important role  
554 in North America, northern South America, Europe, northern Africa, boreal and central  
555 Asia, and Australia. FireMIP models generally simulate increased regional fire  
556 emissions with increased CO<sub>2</sub> concentration and negligible impacts due to changes in  
557 lightning frequency, similar to the responses of global fire emissions.

558

## 559 **5 Summary and outlook**

560 Our study provides the first multi-model reconstructions of global historical fire  
561 emissions for 1700–2012, including carbon and 33 species of trace gases and aerosols.  
562 Two versions of the fire emission product are available, at the original spatial resolution  
563 for outputs of each FireMIP model and on a unified 1x1 degree. The dataset is based on  
564 simulations of fire carbon emissions and vegetation distribution from nine DGVMs  
565 with state-of-the-art global fire models that participated in FireMIP and the most  
566 up-to-date emission factors over various land cover types. It will be available to the  
567 public at <https://zenodo.org/record/3386620#.XXaE1eRYaP8>.

568 Our study provides an important dataset with wide-ranging applications for the  
569 Earth science research community. First, it is the first multi-model-based  
570 reconstruction of fire emissions and can serve as a basis for further development of  
571 multi-source merged products of global and regional fire emissions and of the merging  
572 methodology itself. van Marle et al. (2017b) presented an example for using part of the  
573 dataset to develop a multi-source merged fire emission product as forcing dataset for  
574 CMIP6. In van Marle et al. (2017b), the median of fire carbon emissions from six  
575 FireMIP models was used to determine historical changes over most regions of the  
576 world. The merging method and merged product in van Marle et al. (2017b) are still  
577 preliminary, and need to be improved in the future, e.g., by weighting the different  
578 models depending on their global or regional simulation skills. Secondly, our dataset  
579 includes global gridded reconstructions for 300 years. It can thus be used for  
580 analyzing global and regional historical changes in fire emissions on inter-annual to  
581 multi-decadal time scales and their interplay with climate variability and human  
582 activities. Third, the fire emission reconstructions based on multiple models provide,  
583 for the first time, a chance to quantify and understand the uncertainties in historical  
584 changes of fire emissions and their subsequent impacts on carbon cycle, radiative  
585 balance, air quality, and climate. Hamilton et al. (2018), for example, used fire  
586 emission simulations from two global fire models and the CMIP6 estimates to drive  
587 an aerosol model. This allowed for quantification of the impact of uncertainties in  
588 pre-industrial fire emissions on estimated pre-industrial aerosol concentrations and  
589 historical radiative forcing.

590 This study also provides significant information of the recent state of fire model  
591 performance by evaluating the present-day estimates based on FireMIP fire models  
592 (also those used in the upcoming CMIP6). Our results show that most FireMIP models  
593 can overall reproduce the amount, spatial pattern, and seasonality of fire emissions  
594 shown by satellite-based fire products. Yet they fail to simulate the interannual  
595 variability partly due to a lack of modeling peat and tropical deforestation fires. In  
596 addition, Teckentrup et al. (2019) found that climate was the main driver of  
597 interannual variability for the FireMIP models. A good representation of fire duration  
598 may be important to get the response of fire emissions to climate right. However, all  
599 FireMIP models limit the fire duration of individual fire events no more than one day  
600 in natural vegetation regions, so they cannot skillfully model the drought-induced  
601 large fires that last multiple days (Le Page et al., 2015; Ward et al., 2018). Recently,  
602 Andela et al. (2019) derived a dataset of fire duration from MODIS satellite  
603 observations, which provides a valuable dataset for developing parameterization of  
604 fire duration in global fire models.

605 This study also identifies population density and LULCC as the primary  
606 uncertainty sources in fire emission estimates. Therefore, accurately modeling the  
607 responses to these remains a top priority for reducing uncertainty in historical  
608 reconstructions and future projections of fire emissions, especially given that  
609 modeling is the only way for future projections. For the response to changes in  
610 population density, many FireMIP models have not included the observed relationship  
611 between population density and fire spread (Table 2). Moreover, Bistinas et al. (2014)

612 and Parisien et al. (2016) reported obvious spatial heterogeneity of the population  
613 density–burned area relationship that is poorly represented in FireMIP models.

614 For the response to LULCC, improving the modeling of crop fires, pasture fires,  
615 deforestation and degradation fires, and human indirect effect on fires (e.g.,  
616 fragmentation of the landscape) and reducing the uncertainty in the interpretation of  
617 land use data set in models are critical. Fire has been widely used in agricultural  
618 management during the harvesting, post-harvesting, or pre-planting periods (Korontzi  
619 et al., 2006; Magi et al., 2012). Crop fire emissions are an important source of  
620 greenhouse gases and air pollutants (Tian et al., 2016; Wu et al., 2017; Andreae,  
621 2019). GFED4s reported that fires in croplands can contribute 5% of burned area and  
622 6% of fire carbon emissions globally in the present day (Randerson et al., 2012; van  
623 der Werf et al., 2017). In FireMIP, only CLM4.5 simulates crop fires, whereas the  
624 other models assume no fire in croplands or treat croplands as natural grasslands. In  
625 CLM4.5, crop fires contribute 5% of the global burned area in 2001–2010, similar to  
626 GFED4s estimates. However, CLM4.5 estimates a total of 260 Tg C yr<sup>-1</sup> carbon  
627 emissions (contribution rate:13%), which is higher than the GFED4s estimate (138 Tg  
628 C yr<sup>-1</sup>) because CLM4.5 simulates higher fuel loads in croplands than the CASA  
629 model used by GFED4s. In CLM4.5, both the carbon emissions from crop fires and  
630 the contribution of crop fire emissions to the total fire emissions increase throughout  
631 the 20th century (Fig. S2), which is consistent with earlier estimates based on a  
632 different crop fire scheme (Ward et al., 2018). In JULES-INFERNO, an increase in  
633 cropland area also leads to an increase in burned area and fire carbon emissions

634 because this model treats croplands as natural grasslands. Grasses dry out faster than  
635 woody vegetation and are easier to burn, so an increasing cropland area leads to  
636 increasing burned area and fire carbon emissions. On the other hand, for FireMIP  
637 models that exclude croplands from burning, expansion of croplands leads to a  
638 decrease in burned area and fire carbon emissions. Therefore, different treatment of  
639 crop fires can contribute to the uncertainty in simulated fire emissions. Since four out  
640 of six FireMIP models used for generating CMIP6 estimates exclude croplands from  
641 burning (van Marle et al., 2017b), CMIP6 estimates may underestimate the impact of  
642 historical changes of crop fire emissions in some regions (e.g., China, Russia, India).  
643 Given the small extent of crop fires, high resolution remote sensing may help improve  
644 the detection of crop fires (Randerson et al., 2012; Zhang et al., 2018), which can  
645 benefit the driver analyses and modeling of historical crop fires and their emissions in  
646 DGVMs.

647 Le Page et al. (2017) and Li et al. (2018) highlighted the importance of  
648 tropical deforestation and degradation fires in the long-term changes of reconstructed  
649 and projected global fire emissions, but in FireMIP only CLM4.5 estimates the  
650 tropical deforestation and degradation fires. For pasture fires, all FireMIP models  
651 assume that they behave like natural grassland fires, which needs to be verified by, for  
652 example, satellite-based products. If fires over pastures and natural grasslands are  
653 significantly different, adding the gridded coverage of pasture as a new input field in  
654 DGVMs without pasture PFTs and developing a parameterization of pasture fires will  
655 be necessary. Furthermore, Archibald (2016) and Andela et al. (2017) found that

656 expansion of croplands and pastures decreased fuel continuity and thus reduced  
657 burned area and fire emissions. However, no FireMIP model parameterizes this  
658 indirect human effect on fires. In addition, DGVMs generalize the global vegetation  
659 using different sets of PFTs (Table 4) and represent land use data in different way.  
660 This may lead to different responses of fire emissions to LULCC and thus different  
661 long-term changes of fire emissions among model simulations, given that many  
662 parameters and functions in global fire models are PFT-dependent. LUH2 used in  
663 LUMIP and ongoing CMIP6 provide information of forest/non-forest coverage  
664 changes (Lawrence et al., 2016), which can reduce the misinterpretation of the land  
665 use data in models and thus the inter-model spread of fire emission changes.

666       As discussed above, most FireMIP models do not consider the human  
667 suppression of fire spread, decreased fuel continuity from expanding croplands and  
668 pastures, human deforestation and degradation fires, and crop fires. Therefore, these  
669 models, and hence the CMIP6 estimates that are mainly based on them, may have  
670 some uncertainties in estimating historical fire emissions and long-term trends. This  
671 may further affect the estimates of the radiative forcing of fire emissions and the  
672 historical response of trace gas and aerosol concentrations, temperature, precipitation,  
673 and energy, water, and biogeochemical cycles to fire emissions based on  
674 Earth/climate system models that include these fire models or are driven by such fire  
675 emissions. It may also influence future projections of climate and Earth system  
676 responses to various population density and land use scenarios.

677

678 *Data Availability.* Li, F., Rabin, S. S., Val Martin, M., Hantson, S., Andreae, M. O.,  
679 Arneth, A., Lasslop, G., Yue, C., Bachelet, D., Forrest, M., Kaiser, J. W., Kluzek, E.,  
680 Liu, X., Melton, J. R., Ward, D. S., Darmenov, A., Hickler, T., Ichoku, C., Magi, B. I.,  
681 Sitch, S., van der Werf, G. R., and Wiedinmyer, C.: Model outputs: Historical (1700–  
682 2012) Global Multi-model Estimates of the Fire Emissions from the Fire Modeling  
683 Intercomparison Project (FireMIP) (Version 1.0.1), Zenodo,  
684 <http://doi.org/10.5281/zenodo.3386620>, 2019.

685

686 *Author contribution.* FL contributed to the processing and analyses of the fire  
687 emission dataset. SS and AA designed the FireMIP experiments and LF, SH, GL, CY,  
688 DB, SM, MF, JM, and TH performed FireMIP simulations. MA compiled the EF  
689 table. JK, AD, CI, Gv, CW provided satellite-based and CMIP estimates of fire  
690 emissions. FL prepared the first draft of manuscript, and revised it with contributions  
691 from MVM and other co-authors.

692

693 *Acknowledgements.* This study is co-supported by the National Key R&D Program of  
694 China (2017YFA0604302 and 2017YFA0604804), National Natural Science  
695 Foundation of China (41475099 and 41875137), and CAS Key Research Program of  
696 Frontier Sciences (QYZDY-SSW-DQC002). MVM is supported by the US Joint Fire  
697 Science Program (13-1-01-4) and the UK Leverhulme Trust through a Leverhulme  
698 Research Centre Award (RC-2015-029). AA acknowledges support from the  
699 Helmholtz Association, its ATMO programme and the Impulse and Networking fund



700 which funded initial FireMIP activities. AA and SH acknowledge also the EU FP7  
701 project BACCHUS (603445). GL is funded by the German Research Foundation  
702 (338130981). BIM is supported by NSF (BCS-1436496). CI is supported by NASA  
703 (NNH12ZDA001N-IDS). We are grateful to R. J. Yokelson, Z.-D. Lin, S. Levis, S.  
704 Kloster, M. van Marle, B. Bond-Lamberty, J. R. Marlon, and X. Yue for helpful  
705 discussions. We also thank two anonymous reviewers for their valuable comments  
706 and suggestions, and Editor Qiang Zhang for handling this paper.

707

708 *Competing interests.* The authors declare that they have no conflict of interest.

709

## 710 **References**

- 711 Akagi, S. K., Yokelson, R. J., Wiedinmyer, C., Alvarado, M. J., Reid, J. S., Karl, T.,  
712 Crouse, J. D., and Wennberg, P. O.: Emission factors for open and domestic  
713 biomass burning for use in atmospheric models, *Atmos. Chem. Phys.*, 11, 4039–  
714 4072, <https://doi.org/10.5194/acp-11-4039-2011>, 2011.
- 715 Andela, N., et al.: A human-driven decline in global burned area, *Science*, 356,  
716 1356–1362, 2017.
- 717 Andela, N., Morton, D. C., Giglio, L., Paugam, R., Chen, Y., Hantson, S., van der  
718 Werf, G. R., and Randerson, J. T.: The Global Fire Atlas of individual fire size,  
719 duration, speed and direction, *Earth Syst. Sci. Data*, 11, 529–552,  
720 <https://doi.org/10.5194/essd-11-529-2019>, 2019.
- 721 Andreae, M. O.: Emission of trace gases and aerosols from biomass burning – an  
722 updated assessment, *Atmos. Chem. Phys.*, 19, 8523–8546,

723 <https://doi.org/10.5194/acp-19-8523-2019>, 2019.

724 Andreae, M. O. and Merlet, P.: Emission of trace gases and aerosols from biomass  
725 burning, *Global Biogeochem. Cy.*, 15, 955–966, 2001.

726 Andreae, M. O. and Rosenfeld, D.: Aerosol–cloud– precipitation interactions, Part 1,  
727 The nature and sources of cloud-active aerosols, *Earth-Sci. Rev.*, 89, 13–41,  
728 doi:10.1016/j.earscirev.2008.03.001, 2008.

729 Archibald, S.: Managing the human component of fire regimes: lessons from  
730 Africa, *Philos. T. R. Soc. B.*, 371, 20150346, 2016.

731 Arora, V. K. and Boer, G.: Fire as an interactive component of dynamic vegetation  
732 models, *J. Geophys. Res.*, 110, 2005.

733 Bachelet, K. Ferschweiler, T. J. Sheehan, B. M. Sleeter, and Z. Zhu: Projected carbon  
734 stocks in the conterminous USA with land use and variable fire regimes, *Glob.*  
735 *Change Biol.*, 21, 4548–4560, 2015.

736 Best, M. J., et al.: The Joint UK Land Environment Simulator (JULES), model  
737 description – Part 1: Energy and water fluxes, *Geosci. Model Dev.*, 4, 677–699,  
738 doi:10.5194/gmd-4-677-2011, <http://www.geosci-model-dev.net/4/677/2011/>,  
739 2011.

740 Bistinas, S. P. Harrison, I. C. Prentice, and J. M. C. Pereira: Causal relationships  
741 versus emergent patterns in the global controls of fire frequency, *Biogeosciences*,  
742 11, 5087–5101, 2014.

743 Bond-Lamberty, B., Peckham, S.D., Ahl, D.E., and Gower, S.T.: The dominance of

744 fire in determining carbon balance of the central Canadian boreal forest, *Nature*,  
745 450, 89–92, 2007.

746 Bowman, D. M. J. S., et al.: Fire in the Earth system, *Science*, 324, 481–484, 2009.

747 Brovkin, V., et al.: Effect of anthropogenic land-use and land-cover changes on  
748 climate and land carbon storage in CMIP5 projections for the twenty-first century,  
749 *J. Climate*, 26, 6859–6881, doi:10.1175/JCLI-D-12-00623.1,  
750 <http://journals.ametsoc.org/doi/abs/10.1175/JCLI-D-12-00623.1>, 2013.

751 Chen, Y., Randerson, J., van der Werf, G., Morton, D., Mu, M., and Kasibhatla, P.:  
752 Nitrogen deposition in tropical forests from savanna and deforestation fires, *Glob.*  
753 *Change Biol.*, 16, 2024–2038, 2010.

754 Ciais, P., C., et al.: Carbon and Other Biogeochemical Cycles, In: *Climate Change*  
755 *2013: The Physical Science Basis. Contribution of Working Group I to the Fifth*  
756 *Assessment Report of the Intergovernmental Panel on Climate Change*, edited by:  
757 Stocker, T.F., Qin, D., Plattner, G.-K., Tignor, M., Allen, S.K., Boschung, J.,  
758 Nauels, A., Xia, Y., Bex, V., and Midgley, P. M., Cambridge University Press,  
759 Cambridge, United Kingdom and New York, NY, USA, 467–544, 2013.

760 Clark, D. B. et al.: The Joint UK Land Environment Simulator (JULES), model  
761 description Part 2: Carbon fluxes and vegetation dynamics, *Geosci. Model Dev.*, 4,  
762 701–722, doi:10.5194/gmd-4-701-2011,  
763 <http://www.geosci-model-dev.net/4/701/2011/>, 2011.

764 Conedera, M., Tinner, W., Neff, C., Meurer, M., Dickens, A. F., and Krebs, P.:  
765 Reconstructing past fire regimes: methods, applications, and relevance to fire

766 management and conservation, *Quat. Sci. Rev.*, 28, 555–576,  
767 doi:10.1016/j.quascirev.2008.11.005, 2009.

768 Darmenov, A. S., and da Silva, A.: The Quick Fire Emissions Dataset (QFED):  
769 Documentation of versions 2.1, 2.2 and 2.4, In: Technical Report Series on  
770 Global Modeling and Data Assimilation, edited by Koster, R. D., NASA  
771 Goddard Space Flight Center; Greenbelt, MD, USA, pp. 212, 2015.

772 Falk, D. A., Heyerdahl, E. K., Brown, P. M., Farris, C., Fulé, P. Z., McKenzie, D.,  
773 Swetnam, T. W., Taylor, A. H., and Van Horne, M. L.: Multi-scale controls of  
774 historical forest-fire regimes: new insights from fire-scar networks, *Front. Ecol.*  
775 *Environ.*, 9, 446–454, 2011.

776 Ferretti, D. F., et al. : Unexpected changes to the global methane budget over the past  
777 2000 years, *Science*, 309, 1714–1717, <https://doi.org/10.1126/science.1115193>,  
778 2005.

779 Field, R. D., van der Werf, G. R., and Shen, S. S. P.: Human amplification of  
780 drought-induced biomass burning in Indonesia since 1960, *Nat. Geosci.*, 2, 185–  
781 188, <https://doi.org/10.1038/ngeo443>, 2009.

782 Fisher, J. A., et al.: Source attribution and interannual variability of Arctic pollution in  
783 spring constrained by aircraft (ARCTAS, ARCPAC) and satellite (AIRS)  
784 observations of carbon monoxide, *Atmos. Chem. Phys.*, 10, 977–996,  
785 <https://doi.org/10.5194/acp-10-977-2010>, 2010.

786 Grandey, B. S., Lee, H.-H., and Wang, C.: Radiative effects of interannually varying  
787 vs. interannually invariant aerosol emissions from fires, *Atmos. Chem. Phys.*, 16,

788 14495–14513, <https://doi.org/10.5194/acp-16-14495-2016>, 2016.

789 Hamilton, D. S., et al.: Reassessment of pre-industrial fire emissions strongly affects  
790 anthropogenic aerosol forcing, *Nat. Commun.*, 9, 3182, doi:  
791 10.1038/s41467-018-05592-9, 2018.

792 Hantson, S., Pueyo, S., and Chuvieco, E.: Global fire size distribution is driven by  
793 human impact and climate, *Global Ecol. Biogeogr.*, 24, 77–86, 2015.

794 Hantson, S., et al.: The status and challenge of global fire modelling, *Biogeosciences*,  
795 13, 3359–3375, doi:10.5194/bg-13-3359-2016, 2016.

796 Heymann, J., Reuter, M., Buchwitz, M., Schneising, O., Bovensmann, H., Burrows, J.  
797 P., Massart, S., Kaiser, J. W., and Crisp, D.: CO<sub>2</sub> emission of Indonesian fires in  
798 2015 estimated from satellite-derived atmospheric CO<sub>2</sub> concentrations, *Geophys.  
799 Res. Lett.*, 44, 1537–1544, 2017.

800 Hurtt, G. C., et al.: Harmonization of land-use scenarios for the period 1500–2100:  
801 600 years of global gridded annual land-use transitions, wood harvest, and  
802 resulting secondary lands, *Climatic Change*, 109, 117–161,  
803 doi:10.1007/s10584-011-0153-2, 2011.

804 Ichoku, C. and Ellison, L.: Global top-down smoke-aerosol emissions estimation  
805 using satellite fire radiative power measurements, *Atmos. Chem. Phys.*, 14, 6643–  
806 6667, <https://doi.org/10.5194/acp-14-6643-2014>, 2014.

807 Jiang, Y., Lu, Z., Liu, X. Qian, Y., Zhang, K., Wang, Y., and Yang, X.: Impacts of  
808 global wildfire aerosols on direct radiative, cloud and surface-albedo forcings  
809 simulated with CAM5, *Atmos. Chem. Phys.*, 16, 14805–14824, 2016

810 Johnston, F. H., et al.: Estimated global mortality attributable to smoke from  
811 landscape fires, *Environ. Health Persp.*, 120, 695–701.  
812 <https://doi.org/10.1289/ehp.1104422>, 2012.

813 Kaiser, J. W., Heil, A., Andreae, M. O., Benedetti, A., Chubarova, N., Jones, L.,  
814 Morcrette, J.-J., Razinger, M., Schultz, M. G., Suttie, M., and van der Werf, G. R.:  
815 Biomass burning emissions estimated with a global fire assimilation system based  
816 on observed fire radiative power, *Biogeosciences*, 9, 527–554,  
817 <https://doi.org/10.5194/bg-9-527-2012>, 2012.

818 Keenan, T. F., Hollinger, D. Y., Bohrer, G., Dragoni, D., Munger, J. W., Schmid, H.  
819 P., and Richardson, A. D.: Increase in forest water-use efficiency as atmospheric  
820 carbon dioxide concentrations rise, *Nature*, 499, 324–327, 2013.

821 Klein Goldewijk, K., Beusen, A., and Janssen, P.: Long-term dynamic modeling of  
822 global population and built-up area in a spatially explicit way: HYDE 3.1,  
823 *Holocene*, 20, 565–573, <https://doi.org/10.1177/0959683609356587>, 2010.

824 Kloster, S., and Lasslop, G.: Historical and future fire occurrence (1850 to 2100)  
825 simulated in CMIP5 Earth System Models, *Global Planet. Change*, 58–69, 2017.

826 Kloster, S., Mahowald, N. M., Randerson, J. T., Thornton, P. E., Hoffman, F. M.,  
827 Levis, S., Lawrence, D. M.: Fire dynamics during the 20th century simulated by  
828 the Community Land Model. *Biogeosciences*, 7(6), 1877–1902.  
829 <https://doi.org/10.5194/bg-7-1877-2010>, 2010.

830 Knorr, W., Jiang, L., and Arneth, A.: Climate, CO<sub>2</sub> and human population impacts on  
831 global wildfire emissions, *Biogeosciences*, 13, 267–282,

832 <https://doi.org/10.5194/bg-13-267-2016>, 2016.

833 Knorr, W., Dentener, F., Lamarque, J.-F., Jiang, L., and Arneeth, A.: Wildfire air  
834 pollution hazard during the 21st century, *Atmos. Chem. Phys.*, 17, 9223–9236,  
835 <https://doi.org/10.5194/acp-17-9223-2017>, 2017.

836 Kondo, M., et al.: Land use change and El Niño-Southern Oscillation drive decadal  
837 carbon balance shifts in Southeast Asia, *Nat. Commun.*, 9, 1154, doi:  
838 10.1038/s41467-018-03374-x, 2018.

839 Konovalov, I. B., Berezin, E. V., Ciais, P., Broquet, G., Beekmann, M., Hadji- Lazaro,  
840 J., Clerbaux, C., Andreae, M. O., Kaiser, J. W., and Schulze, E.: Constraining  
841 CO<sub>2</sub> emissions from open biomass burning by satellite observations of co-emitted  
842 species: a method and its application to wildfires in Siberia, *Atmos. Chem. Phys.*,  
843 14, 10383–10410, 2014.

844 Konovalov, I. B., Lvova, D. A., Beekmann, M., Jethva, H., Mikhailov, E. F., Paris,  
845 J.-D., Belan, B. D., Kozlov, V. S., Ciais, P., and Andreae, M. O.: Estimation of  
846 black carbon emissions from Siberian fires using satellite observations of  
847 absorption and extinction optical depths, *Atmos. Chem. Phys.*, 18, 14889–14924,  
848 <https://doi.org/10.5194/acp-18-14889-2018>, 2018.

849 Korontzi, S., McCarty, J., Loboda, T., Kumar, S., and Justice, C.: Global distribution  
850 of agricultural fire in croplands from 3 years of Moderate Resolution Imaging  
851 Spectroradiometer (MODIS) data, *Global Biogeochem. Cy.*, 20, GB2021,  
852 doi:10.1029/2005GB002529, 5 2006.

853 Krinner, G., Viovy, N., de Noblet-Ducoudré, N., Ogée, J., Polcher, J., Friedlingstein,

854 P., Ciais, P., Sitch, S., and Prentice, I. C.: A dynamic global vegetation model for  
855 studies of the coupled atmosphere-biosphere system, *Global Biogeochem. Cy.*, 19,  
856 1–33, <https://doi.org/10.1029/2003GB002199>, 2005.

857 Krol, M., Peters, W., Hooghiemstra, P., George, M., Clerbaux, C., Hurtmans, D.,  
858 McInerney, D., Sedano, F., Bergamaschi, P., El Hajj, M., Kaiser, J. W., Fisher, D.,  
859 Yershov, V., and Muller, J.-P.: How much CO was emitted by the 2010 fires  
860 around Moscow? *Atmos. Chem. Phys.*, 13(9):4737–4747, 2013.

861 Lamarque, J.-F., et al.: Historical (1850–2000) gridded anthropogenic and biomass  
862 burning emissions of reactive gases and aerosols: methodology and application,  
863 *Atmos. Chem. Phys.*, 10, 7017–7039, <https://doi.org/10.5194/acp-10-7017-2010>,  
864 2010.

865 Lasslop, G., Thonicke, K., and Kloster, S.: SPITFIRE within the MPI Earth system  
866 model: Model development and evaluation, *J. Adv. Model Earth Sy.*, 6, 740–755,  
867 <https://doi.org/10.1002/2013MS000284>, 2014.

868 Lawrence, D. M., et al.: The Land Use Model Intercomparison Project (LUMIP)  
869 contribution to CMIP6: rationale and experimental design, *Geosci. Model Dev.*, 9,  
870 2973–2998, <https://doi.org/10.5194/gmd-9-2973-2016>, 2016.

871 Legrand, M., et al.: Boreal fire records in Northern Hemisphere ice cores: a review,  
872 *Clim. Past*, 12, 2033–2059, <https://doi.org/10.5194/cp-12-2033-2016>, 2016.

873 Lehsten, V., Tansey, K., Balzter, H., Thonicke, K., Spessa, A., Weber, U., Smith, B.,  
874 and Arneeth, A.: Estimating carbon emissions from African wildfires,  
875 *Biogeosciences*, 6, 349–360, <https://doi.org/10.5194/bg-6-349-2009>, 2009.



876 Lelieveld, J., Evans, J. S., Fnais, M., Giannadaki, D., and Pozzer, A.: The con-  
877 tribution of outdoor air pollution sources to premature mortality on a global scale,  
878 *Nature*, 525, 367– 371, 2015.

879 Le Page, Y., Morton, D., Bond-Lamberty, B., Pereira, J. M. C., and Hurtt, G.:  
880 HESFIRE: A global fire model to explore the role of anthropogenic and weather  
881 drivers, *Biogeosciences*, 12, 887–903, <https://doi.org/10.5194/bg-12-887-2015>,  
882 2015.

883 Le Page, Y., Morton, D., Hartin, C., Bond-Lamberty, B., Pereira, J. M. C., Hurtt, G.,  
884 and Asrar, G.: Synergy between land use and climate change increases future fire  
885 risk in Amazon forests, *Earth Syst. Dynam.*, 8, 1237–1246,  
886 <https://doi.org/10.5194/esd-8-1237-2017>, 2017.

887 Le Quéré, C., et al.: Global carbon budget 2013, *Earth Syst. Sci. Data*, 6, 235–263,  
888 [doi:10.5194/essd-6-235-2014](https://doi.org/10.5194/essd-6-235-2014), <http://www.earth-syst-sci-data.net/6/235/2014/>,  
889 2014.

890 Levis, S., Bonan, G. B., Vertenstein, M., and Oleson, K. W.: The Community Land  
891 Model’s dynamic global vegetation model (CLM-DGVM): Technical description  
892 and user’s guide, NCAR Tech. Note TN-459 IA, Terrestrial Sciences Section,  
893 Boulder, Colorado, 2004.

894 Li, F., and Lawrence, D. M.: Role of fire in the global land water budget during the  
895 20th century through changing ecosystems, *J. Clim.*, 30, 1893–908, 2017.

896 Li, F., Zeng, X.-D., Levis, S.: A process-based fire parameterization of intermediate  
897 complexity in a Dynamic Global Vegetation Model, *Biogeosciences*, 9, 2761–  
898 2780, 2012.

899 Li, F., Levis, S., and Ward, D. S.: Quantifying the role of fire in the Earth system–Part  
900 1: Improved global fire modeling in the Community Earth System Model  
901 (CESM1), *Biogeosciences*, 10, 2293–2314, 2013.

902 Li, F., Lawrence, D.M., Bond-Lamberty, B.: Human impacts on 20th century fire  
903 dynamics and implications for global carbon and water trajectories, *Glob. Planet.*  
904 *Change*, 162, 18–27, 2018.

905 Lindeskog, M., Arneth, A., Bondeau, A., Waha, K., Seaquist, J., Olin, S., and Smith,  
906 B.: Implications of accounting for land use in simulations of ecosystem carbon  
907 cycling in Africa, *Earth Syst. Dynam.*, 4, 385–407, doi:10.5194/esd-4-385-2013,  
908 2013.

909 Magi, B.I., Rabin, S., Shevliakova, E., Pacala, S.: Separating agricultural and  
910 non-agricultural fire seasonality at regional scales, *Biogeosciences*, 9,  
911 3003–3012, 2012.

912 Mahowald, N., et al.: Global distribution of atmospheric phosphorus sources,  
913 concentrations and deposition rates, and anthropogenic impacts, *Global*  
914 *Biogeochem. Cy.*, 22, GB4026, doi: 10.1029/2008GB003240, 2008.

915 Mangeon, S., Voulgarakis, A., Gilham, R., Harper, A., Sitch, S., and Folberth, G.:  
916 INFERNO: a fire and emissions scheme for the UK Met Office’s Unified Model,  
917 *Geosci. Model Dev.*, 9, 2685–2700, doi:10.5194/gmd-9-2685-2016,

918 <http://www.geosci-model-dev.net/9/2685/2016/>, 2016.

919 Mao, J. F., Wang, B., and Dai, Y. J.: Sensitivity of the carbon storage of potential  
920 vegetation to historical climate variability and CO<sub>2</sub> in continental China, *Adv.*  
921 *Atmos. Sci.*, 26, 87–100, 2009.

922 Marlier, M. E., DeFries, R. S., Voulgarakis, A., Kinney, P. L., Randerson, J. T.,  
923 Shindell, D. T., Chen, Y., and Faluvegi, G.: El Niño and health risks from  
924 landscape fire emissions in southeast Asia, *Nat. Clim. Change*, 3, 131–136, 2013.

925 Marlon, J. R., et al.: Climate and human influences on global biomass  
926 burning over the past two millennia, *Nat. Geosci.*, 1, 697–702,  
927 <https://doi.org/10.1038/ngeo313>, 2008.

928 Marlon, J. R., et al.: Reconstructions of biomass burning from sediment–charcoal  
929 records to improve data–model comparisons, *Biogeosciences*, 13, 3225–3244,  
930 <https://doi.org/10.5194/bg-13-3225-2016>, 2016.

931 McKendry, I. G., Christen, A., Lee, S.-C., Ferrara, M., Strawbridge, K. B., O'Neill, N.,  
932 and Black, A.: Impacts of an intense wildfire smoke episode on surface radiation,  
933 energy and carbon fluxes in southwestern British Columbia, Canada, *Atmos.*  
934 *Chem. Phys.*, 19, 835–846, <https://doi.org/10.5194/acp-19-835-2019>,  
935 2019. McConnell, J. R., Edwards, R., Kok, G. L., Flanner, M. G., Zender, C. S.,  
936 Saltzman, E. S., Banta, J. R., Pasteris, D. R., Carter, M. M., and Kahl, J. D. W.:  
937 20th-century industrial black carbon emissions altered arctic climate forcing,  
938 *Science*, 317, 1381–1384, doi:10.1126/science.1144856, 2007.

939 Melton, J. R., and Arora, V. K.: Competition between plant functional types in the

940 Canadian Terrestrial Ecosystem Model (CTEM) v. 2.0, *Geosci. Model Dev.*, 9,  
941 323–361, doi:10.5194/gmd-9-323-2016, 2016.

942 Mieville, A., Granier, C., Lioussé, C., Guillaume, B., Mouillot, F., Lamarque, J.-F.,  
943 Grégoire, J.-M., and Pétron, G.: Emissions of gases and particles from biomass  
944 burning during the 20th century using satellite data and an historical  
945 reconstruction, *Atmos. Environ.*, 44, 1469–1477,  
946 <https://doi.org/10.1016/j.atmosenv.2010.01.011>, 2010.

947 Mouillot, F. and Field, C. B.: Fire history and the global carbon budget: a 1°×1°fire  
948 history reconstruction for the 20th century, *Glob. Change Biol.*, 11, 398–420,  
949 <https://doi.org/10.1111/j.1365-2486.2005.00920.x>, 2005.

950 Nemani, R.R., and Running, S.W.: Implementation of a hierarchical global vegetation  
951 classification in ecosystem function models, *J. Veg. Sci.*, 7, 337–346, 1996.

952 Oleson, K., et al.: Technical Description of version 4.5 of the Community Land  
953 Model (CLM), Tech. Rep. NCAR/TN-503+STR NCAR, Boulder, CO, USA,  
954 pp.434, 2013.

955 Parisien, M., Miller, C., Parks, S.A., DeLancey, E.R., Robinne, F., and Flannigan, M.  
956 D.: The spatially varying influence of humans on fire probability in North  
957 America, *Environ. Res. Lett.*, 11:075005, 2016.

958 Pechony, O., and Shindell, D.T.: Driving forces of global wildfires over the past  
959 millennium and the forthcoming century, *P. Natl. Acad. Sci. USA*, 107,  
960 19167–19170, 2010.

961 Pfeiffer, M., Spessa, A., and Kaplan, J. O.: A model for global biomass burning in

962 preindustrial time: LPJ-LMfire (v1.0), *Geosci. Model Dev.*, 6, 643–685,  
963 doi:10.5194/gmd-6-643-2013, 2013.

964 Rabin, S. S., et al.: The Fire Modeling Intercomparison Project (FireMIP),  
965 phase 1: experimental and analytical protocols with detailed model descriptions.  
966 *Geosci. Model Dev.*, 10, 1175–1197, 2017.

967 Rabin, S. S., Ward, D. S., Malyshev, S. L., Magi, B. I., Shevliakova, E., and Pacala, S.  
968 W.: A fire model with distinct crop, pasture, and non-agricultural burning: use of  
969 new data and a model-fitting algorithm for FINAL.1, *Geosci. Model Dev.*, 11,  
970 815–842, <https://doi.org/10.5194/gmd-11-815-2018>, 2018.

971 Reddington, C. L., Morgan, W. T., Darbyshire, E., Brito, J., Coe, H., Artaxo, P., Scott,  
972 C. E., Marsham, J., and Spracklen, D. V.: Biomass burning aerosol over the  
973 Amazon: analysis of aircraft, surface and satellite observations using a global  
974 aerosol model, *Atmos. Chem. Phys.*, 19, 9125–9152,  
975 <https://doi.org/10.5194/acp-19-9125-2019>, 2019.

976 Randerson, J. T., Chen, Y., van der Werf, G. R., Rogers, B. M., and Morton, D. C.:  
977 Global burned area and biomass burning emissions from small fires, *J. Geophys.*  
978 *Res.*, 117, G04012, <https://doi.org/10.1029/2012JG002128>, 2012. Rothermel, R. C.:  
979 A mathematical model for predicting fire spread in wildland fuels, Res. Pap.  
980 INT-115, US Department of Agriculture, Ogden, UT, USA, pp. 40, 1972.

981 Schultz, M. G., Heil, A., Hoelzemann, J. J., Spessa, A., Thonicke, K., Goldammer, J.  
982 G., Held, A. C., Pereira, J. M. C., and van het Bolscher, M.: Global wildland fire  
983 emissions from 1960 to 2000, *Global Biogeochem. Cy.*, 22, GB2002,

984 <https://doi.org/10.1029/2007GB003031>, 2008.

985 Scott, A. C., and Glasspool, I. J.: The diversification of Palaeozoic fire systems and  
986 fluctuations in atmospheric oxygen concentration, *Proc. Natl. Acad. Sci. U.S.A.*,  
987 103, 10861–10865, doi:10.1073/pnas.0604090103, 2006.

988 Sheehan, T., Bachelet, D., and Ferschweiler, K.: Projected major fire and vegetation  
989 changes in the Pacific Northwest of the conterminous United States under  
990 selected CMIP5 climate futures, *Ecol. Model.*, 317, 16–29,  
991 doi:10.1016/j.ecolmodel.2015.08.023, 2015.

992 Smith, B., Wårlind, D., Arneth, A., Hickler, T., Leadley, P., Siltberg, J., and Zaehle,  
993 S.: Implications of incorporating N cycling and N limitations on primary  
994 production in an individual-based dynamic vegetation model, *Biogeosciences*, 11,  
995 2027–2054, doi:10.5194/bg-11-2027-2014, 2014.

996 Stockwell, C. E., et al.: Nepal Ambient Monitoring and Source Testing Experiment  
997 (NAMaSTE): emissions of trace gases and light-absorbing carbon from wood and  
998 dung cooking fires, garbage and crop residue burning, brick kilns, and other  
999 sources, *Atmos. Chem. Phys.*, 16, 11043-11081, 2016.

1000 Thonicke, K., Venevsky, S., Sitch, S., and Cramer, W.: The role of fire disturbance  
1001 for global vegetation dynamics: Coupling fire into a Dynamic Global Vegetation  
1002 Model, *Global Ecol. Biogeogr.*, 10, 661–677, 2001.

1003 Thonicke, K., Spessa, A., Prentice, I. C., Harrison, S. P., Dong, L., and  
1004 Carmona-Moreno, C.: The influence of vegetation, fire spread and fire behaviour  
1005 on biomass burning and trace gas emissions: Results from a process-based model,

1006 Biogeosciences, 7, 1991–2011, 2010.

1007 Thornhill, G. D., Ryder, C. L., Highwood, E. J., Shaffrey, L. C., and Johnson, B. T.:

1008 The effect of South American biomass burning aerosol emissions on the regional

1009 climate, *Atmos. Chem. Phys.*, 18, 5321–5342,

1010 <https://doi.org/10.5194/acp-18-5321-2018>, 2018.

1011 Tian, H., et al.: The terrestrial biosphere as a net source of greenhouse gases to the

1012 atmosphere, *Nature*, 531, 225–228, 2016.

1013 Tosca, M. G., Randerson, J. T., and Zender, C. S.: Global impact of smoke aerosols

1014 from landscape fires on climate and the Hadley circulation, *Atmos. Chem. Phys.*,

1015 13, 5227–5241, <https://doi.org/10.5194/acp-13-5227-2013>, 2013.

1016 Teckentrup, L., Harrison, S. P., Hantson, S., Heil, A., Melton, J. R., Forrest, M., Li, F.,

1017 Yue, C., Arneth, A., Hickler, T., Sitch, S., and Lasslop, G.: Sensitivity of

1018 simulated historical burned area to environmental and anthropogenic controls: A

1019 comparison of seven fire models, *Biogeosciences Discuss.*,

1020 <https://doi.org/10.5194/bg-2019-42>, 2019.

1021 Val Martin, M., Heald, C.L., Lamarque, J.F., Tilmes, S., Emmons, L.K., Schichtel,

1022 B.A.: How emissions, climate, and land use change will impact mid-century air

1023 quality over the United States: a focus on effects at national parks, *Atmos. Chem.*

1024 *Phys.* 15, 2805–2823, 2015.

1025 van der Werf, G. R., Randerson, J. T., Giglio, L., Collatz, G. J., Kasibhatla, P. S., and

1026 Arellano Jr., A. F.: Interannual variability in global biomass burning emissions

1027 from 1997 to 2004, *Atmos. Chem. Phys.*, 6, 3423–3441,  
1028 <https://doi.org/10.5194/acp-6-3423-2006>, 2006.

1029 van der Werf, G. R., Randerson, J. T., Giglio, L., Collatz, G. J., Mu, M., Kasibhatla,  
1030 P. S., Morton, D. C., DeFries, R. S., Jin, Y., and van Leeuwen, T. T.: Global fire  
1031 emissions and the contribution of deforestation, savanna, forest, agricultural, and  
1032 peat fires (1997–2009), *Atmos. Chem. Phys.*, 10, 11707–11735,  
1033 <https://doi.org/10.5194/acp-10-11707-2010>, 2010.

1034 van der Werf, G. R., Peters, W., van Leeuwen, T. T., and Giglio, L.: What could have  
1035 caused pre-industrial biomass burning emissions to exceed current rates?, *Clim.*  
1036 *Past*, 9, 289–306, <http://www.clim-past.net/9/289/2013/>, 2013.

1037 van der Werf, G. R., et al.: Global fire emissions estimates during 1997–2016, *Earth*  
1038 *Syst. Sci. Data.*, 9, 679–720, 2017.

1039 van Marle, M. J. E., Field, R. D., van der Werf, G. R., Estrada de Wagt, I. A.,  
1040 Houghton, R. A., Rizzo, L. V., Artaxo, P., and Tsigaridis, K.: Fire and  
1041 deforestation dynamics in Amazonia (1973–2014), *Global Biogeochem. Cy.*, 31,  
1042 24–38, <https://doi.org/10.1002/2016GB005445>, 2017a.

1043 van Marle, M. J. E., et al., Historic global biomass burning emissions based on  
1044 merging satellite observations with proxies and fire models (1750–2015), *Geosci.*  
1045 *Model Dev.*, 10, 3329–3357, doi:10.5194/gmd-2017-32, 2017b.

1046 Wang, Z., et al.: The isotopic record of Northern Hemisphere atmospheric carbon  
1047 monoxide since 1950: implications for the CO budget, *Atmos. Chem. Phys.*, 12,  
1048 4365–4377, <https://doi.org/10.5194/acp-12-4365-2012>, 2012.



1049 Ward, D. S., Kloster, S., Mahowald, N. M., Rogers, B.M., Randerson, J. T., Hess, P.  
1050 G.: The changing radiative forcing of fires: Global model estimates for past,  
1051 present and future, *Atmos. Chem. Phys.* 12, 10857–10886, 2012.

1052 Ward, D. S., Shevliakova, E., Malyshev, S., Rabin, S.: Trends and variability  
1053 of global fire emissions due to historical anthropogenic activities. *Global*  
1054 *Biogeochem. Cy.*,32, 122–142, <https://doi.org/10.1002/2017GB005787>,  
1055 2018.

1056 Wei, Y., et al.: The North American Carbon Program Multi-scale Synthesis and  
1057 Terrestrial Model Intercomparison Project – Part 2: Environmental driver data,  
1058 *Geoscientific Model Development*, 7, 2875–2893, doi:10.5194/gmd-7-2875-2014,  
1059 2014.

1060 Wiedinmyer, C., Akagi, S. K., Yokelson, R. J., Emmons, L. K., Al-Saadi, J. A.,  
1061 Orlando, J. J., and Soja, A. J. : The Fire INventory from NCAR (FINN): A high  
1062 resolution global model to estimate the emissions from open burning, *Geosci.*  
1063 *Model Dev.*, 4, 625–641, <https://doi.org/10.5194/gmd-4-625-2011>, 2011

1064 Wu, Y., Han, Y., Voulgarakis, A., Wang, T., Li, M., Wang, Y., Xie, M., Zhuang, B.,  
1065 and Li, S.: An agricultural biomass burning episode in eastern China: Transport,  
1066 optical properties, and impacts on regional air quality, *J. Geophys. Res.-Atmos.*,  
1067 122, 2304–2324, doi:10.1002/2016JD025319, 2017.

1068 Yang, J., Tian, H., Tao, B., Ren, W., Kush, J., Liu, Y., and Wang, Y.: Spatial and  
1069 temporal patterns of global burned area in response to anthropogenic and  
1070 environmental factors: Reconstructing global fire history for the 20th and early

1071 21st centuries, *J. Geophys. Res., -Biogeo.*, 119, 249–263.  
1072 <https://doi.org/10.1002/2013JG002532>, 2014.

1073 Yokelson, R. J., et al.: Coupling field and laboratory measurements to estimate the  
1074 emission factors of identified and unidentified trace gases for prescribed fires,  
1075 *Atmos. Chem. Phys.*, 13, 89–116, doi:10.5194/acp-13-89-2013, 2013.

1076 Yue, C., et al.: Modelling the role of fires in the terrestrial carbon balance by  
1077 incorporating SPITFIRE into the global vegetation model ORCHIDEE – Part 1:  
1078 simulating historical global burned area and fire regimes, *Geosci. Model Dev.*, 7,  
1079 2747–2767, <https://doi.org/10.5194/gmd-7-2747-2014>, 2014.

1080 Yue, C., Ciais, P., Cadule, P., Thonicke, K., and van Leeuwen, T. T.: Modelling the  
1081 role of fires in the terrestrial carbon balance by incorporating SPITFIRE into the  
1082 global vegetation model ORCHIDEE– Part 2: Carbon emissions and the role of  
1083 fires in the global carbon balance, *Geosci. Model Dev.*, 8, 1321–1338,  
1084 <https://doi.org/10.5194/gmd-8-1321-2015>, 2015.

1085 Yue, X., and Unger, N.: Fire air pollution reduces global terrestrial productivity,  
1086 *nature commun.*, 9, 5413, <https://doi.org/10.1038/s41467-018-07921-4>, 2018.

1087 Zennaro, P., et al.: Fire in ice: two millennia of boreal forest fire history from the  
1088 Greenland NEEM ice core, *Clim. Past*, 10, 1905–1924,  
1089 <https://doi.org/10.5194/cp-10-1905-2014>, 2014.

1090 Zhang, F., Wang, J., Ichoku, C., Hyer, E. J., Yang, Z., Ge, C., Su, S., Zhang, X.,  
1091 Kondragunta, S., Kaiser, J. W., Wiedinmyer, C., and da Silva, A.: Sensitivity of  
1092 mesoscale modeling of smoke direct radiative effect to the emission inventory: a

1093 case study in northern sub-Saharan African region, *Environ. Res. Lett.*, 9, 075002,  
1094 doi:10.1088/1748-9326/9/7/075002, 2014.

1095 Zhang, T. R., Wooster, M. J., de Jong, M. C., and Xu, W. D.: How well does the  
1096 ‘Small Fire Boost’ methodology used within the GFED4.1s fire emissions  
1097 database represent the timing, location and magnitude of agricultural burning?  
1098 *Remote. Sens.*, 10, 823, doi:10.3390/rs10060823, 2018.

1099 Zhu, Z., et al: Greening of the Earth and its drivers, *Nat. Clim. Change*, 6, 791–795,  
1100 2016.

**Table 1.** Summary description of the Dynamic Global Vegetation Models (DGVMs)

participated in FireMIP.

DGVMs	tem. res. of model outputs	spatial res. of model outputs	period	natural veg. distrib.	fire scheme ref.	DGVM ref.
CLM4.5 but CLM5 fire model (CLM4.5)	monthly	~1.9° (lat) ×2.5° (lon)	1700– 2012	P	Li et al. (2012, 2013) Li and Lawrence (2017)	Oleson et al. (2013)
CTEM	monthly	2.8125°	1861– 2012	P	Arora and Boer (2005) Melton and Arora (2016)	Melton and Arora (2016)
JSBACH-SPITFIRE (JSBACH)	monthly	1.875°	1700– 2012	P	Lasslop et al. (2014) Thonicke et al. (2010)	Brovkin et al. (2013)
JULES-INFERNO (JULES)	monthly	~1.2° (lat) ×1.9°(lon)	1700– 2012	M	Mangeon et al. (2016)	Best et al. (2011) Clark et al. (2011)
LPJ-GUESS-GlobFIRM (LGG)	annual	0.5°	1700– 2012	M	Thonicke et al. (2001)	Smith et al. (2014) Lindeskog et al. (2013)
LPJ-GUESS-SPITFIRE (LGS)	monthly	0.5°	1700– 2012	M	Lehsten et al. (2009) Rabin et al. (2017)	Smith et al. (2001) Ahlstrom et al. (2012)
LPJ-GUESS-SIMFIRE -BLAZE (LGSB)	monthly	0.5°	1700– 2012	M	Knorr et al. (2016)	Smith et al. (2014) Lindeskog et al. (2013) Nieradzick et al. (2017)
MC2	annual	0.5°	1901– 2008	M	Bachelet et al. (2015) Sheehan et al. (2015)	Bachelet et al. (2015) Sheehan et al. (2015)
ORCHIDEE-SPITFIRE (ORCHIDEE)	monthly	0.5°	1700– 2012	P	Yue et al. (2014, 2015) Thonicke et al. (2010)	Krinner et al. (2005)

Acronyms: CLM4.5 and CLM5: Community Land Model version 4.5 and 5; CTEM: Canadian Terrestrial Ecosystem Model; JSBACH: Jena Scheme for Biosphere-Atmosphere Coupling in Hamburg; SPITFIRE: Spread and InTensity fire model; JULES: Joint UK Land Environment Simulator; INFERNO: Interactive Fire And Emission Algorithm For Natural Environments; GlobFIRM: fire module Global FIRE Model; SMIFIRE: SIMple FIRE model; BLAZE: Blaze-Induced Land-Atmosphere Flux Estimator; ORCHIDEE: Organizing Carbon Hydrology In Dynamic Ecosystems; PFT: plant functional type; P: prescribed; M: modeled

**Table 2.** Summary description of global fire modules in FireMIP DGVMs.

DGVMs	crop fire	tropical human defor. fire	human ignition	human fire suppression	peat fire	pasture	combust. complete. range of woody tissue
CLM4.5	yes	yes	increase with PD <sup>a</sup>	occurrence & spread area <sup>b</sup>	yes <sup>e</sup>	as natural grassland	27–35% (stem) 40% (CWD <sup>f</sup> )
CTEM	no	no	increase with PD	occurrence & duration <sup>c</sup>	no	as natural grassland	6% (stem) 15–18% (CWD)
JSBACH	as grass fire	no	increase with PD	occurrence & duration <sup>c</sup>	no	high fuel bulk den.	0–45%
JULES	no	no	increase with PD	occurrence <sup>c</sup>	no	as natural grassland	0–40%
LGG	no	no	no	no	no	harvest	70–90%
LGS	no	no	increase with PD	occurrence <sup>c</sup>	no	as natural grassland	0–98% (100h <sup>g</sup> ) 0–80% (1000h <sup>g</sup> )
LGSB	no	no	increase with PD	burned area <sup>c</sup>	no	harvest	0–50%
MC2	no	no	no	occurrence <sup>d</sup>	no	as natural grassland	0–87% (100h) 0–43% (1000h)
ORCHIDEE	no	no	increase with PD	occurrence <sup>c</sup>	no	as natural grassland	0–73% (100h) 0–41% (1000h)

<sup>a</sup> PD: population density

<sup>b</sup> fire suppression increases with PD and GDP, different between tree PFTs and grass/shrub PFTs

<sup>c</sup> fire suppression increases with PD

<sup>d</sup> Assume no fire in grid cell when pre-calculated rate of spread, fireline intensity, and energy release component are lower than thresholds

<sup>e</sup> CLM4.5 outputs in FireMIP include biomass and litter burning due to peat fires, but don't include burning of soil organic matter

<sup>f</sup> Coarse Woody Debris

<sup>g</sup> 100-hour fuels and 1000-hour fuel classes

**Table 3.** Emission factors (g species (kg DM)<sup>-1</sup>) for land cover types (LCTs).

No.	Species	grassland /savanna	tropical forest	temperate forest	boreal forest	cropland
1	CO <sub>2</sub>	1647	1613	1566	1549	1421
2	CO	70	108	112	124	78
3	CH <sub>4</sub>	2.5	6.3	5.8	5.1	5.9
4	NMHC	5.5	7.1	14.6	5.3	5.8
5	H <sub>2</sub>	0.97	3.11	2.09	1.66	2.65
6	NO <sub>x</sub>	2.58	2.55	2.90	1.69	2.67
7	N <sub>2</sub> O	0.18	0.20	0.25	0.25	0.09
8	PM <sub>2.5</sub>	7.5	8.3	18.1	20.2	8.5
9	TPM	8.5	10.9	18.1	15.3	11.3
10	TPC	3.4	6.0	8.4	10.6	5.5
11	OC	3.1	4.5	8.9	10.1	5.0
12	BC	0.51	0.49	0.66	0.50	0.43
13	SO <sub>2</sub>	0.51	0.78	0.75	0.75	0.81
14	C <sub>2</sub> H <sub>6</sub> (ethane)	0.42	0.94	0.71	0.90	0.76
15	CH <sub>3</sub> OH (methanol)	1.48	3.15	2.13	1.53	2.63
16	C <sub>3</sub> H <sub>8</sub> (propane)	0.14	0.53	0.29	0.28	0.20
17	C <sub>2</sub> H <sub>2</sub> (acetylene)	0.34	0.43	0.35	0.27	0.32
18	C <sub>2</sub> H <sub>4</sub> (ethylene)	1.01	1.11	1.22	1.49	1.14
19	C <sub>3</sub> H <sub>6</sub> (propylene)	0.49	0.86	0.67	0.66	0.48
20	C <sub>5</sub> H <sub>8</sub> (isoprene)	0.12	0.22	0.19	0.07	0.18
21	C <sub>10</sub> H <sub>16</sub> (terpenes)	0.10	0.15	1.07	1.53	0.03
22	C <sub>7</sub> H <sub>8</sub> (toluene)	0.20	0.23	0.43	0.32	0.18
23	C <sub>6</sub> H <sub>6</sub> (benzene)	0.34	0.38	0.46	0.52	0.31
24	C <sub>8</sub> H <sub>10</sub> (xylene)	0.09	0.09	0.17	0.10	0.09
25	CH <sub>2</sub> O (formaldehyde)	1.33	2.40	2.22	1.76	1.80
26	C <sub>2</sub> H <sub>4</sub> O (acetaldehyde)	0.86	2.26	1.20	0.78	1.82
27	C <sub>3</sub> H <sub>6</sub> O (acetone)	0.47	0.63	0.70	0.61	0.61
28	C <sub>3</sub> H <sub>6</sub> O <sub>2</sub> (hydroxyacetone)	0.52	1.13	0.85	1.48	1.74
29	C <sub>6</sub> H <sub>5</sub> OH (Phenol)	0.37	0.23	0.33	2.96	0.50
30	NH <sub>3</sub> (ammonia)	0.91	1.45	1.00	2.82	1.04
31	HCN (hydrogen cyanide)	0.42	0.38	0.62	0.81	0.43
32	MEK/2-butanone	0.13	0.50	0.23	0.15	0.60
33	CH <sub>3</sub> CN (acetonitrile)	0.17	0.51	0.23	0.30	0.25

**Table 4.** Attribution of plant function types (PFTs) in FireMIP DGVMs to land cover types (LCTs) for emission factors described in Table 2.

LCT Models	Grassland /Savannas	Tropical Forest	Temperate Forest	Boreal Forest	Cropland
CLM4.5	A C3/C3/C4 G	Tro BE T	Tem NE T	Bor NE T	Crop
	Bor BD S	Tro BD T	Tem BE T	Bor ND T	
	Tem BE/BD S		Tem BD T	Bor BD T	
CTEM	C3/C4 G	BE T <sup>a</sup>	NE/BE T <sup>a</sup>	NET <sup>a</sup> , ND T	C3/C4 Crop
		Other BD T <sup>a</sup>	Other BD T <sup>a</sup>	Cold BD T	
JSBACH	C3/C4 G/P	Tro E/D T	Ex-Tro E/D T <sup>a</sup>	Ex-Tro E/D T <sup>a</sup>	Crop
JULES	C3/C4 G	Tro BE T	Tem BE T	BD/NE T <sup>a</sup>	
		E/D S	BD T <sup>a</sup>	BD/NE T <sup>a</sup>	
LGG <sup>b</sup>	C3/C4 G	Tro BE/BR T	Tem NSG/BSG/BE T	Bor NE T	R/I S/W Wheat
	C3/C4 G in P	Tro SI BE T	Tem SI SG B T	Bor SI NE T	R/I Maize
LGS	C3/C4 G	Tro BE/BR T	Tem SI/&SG B T	Bor NE T	
		Tro SI BE T	Tem B/N E T	Bor SI/&SG NE/N T	
LGSB <sup>b</sup>	C3/C4 G	Tro BE/BR T	Tem NSG/BSG/ BE T	Bor NE T	R/I S/W Wheat
	C3/C4 G in P	Tro SI BE T	Tem SI SG B T	Bor SI NE T	R/I Maize
MC2	Tem C3 G/S	Tro BE T	Maritime NE F	Bor NE F	
	Sub-Tro C4 G/S	Tro D W <sup>c</sup>	Sub-Tro NE/BD/BE/M F	Subalpine F	
	Tro S/G/Sava		Tem NE/BD F	Cool N F	
	Bor M W		Tem C/W M F		
	Tem/Sub-Tro				
	NE/B/M W				
ORCHIDEE	C3/C4 G	Tro B E/R T	Tem N/B E T	Bor N E/D T	C3/C4 Crop
			Tem BD T	Bor BT T	

Acronyms: T: tree; S: shrub; W: woodland; F: forest; G: grass; P: pasture; Sava: Savanna; N: needleleaf; E: evergreen; B: broadleaf; D: deciduous; R: raingreen; SI: shaded-intolerant; SG: summer-green; M: mixed; I: irrigated; RF: rainfed; C/W: cool or warm; S/W: spring or winter, Tro: Tropical; Tem: Temperate; Bor: Boreal; Sub-Tro: subtropical; Ex-Tro: Extratropical; A: Arctic

<sup>a</sup> split tree PFTs into tropical, temperate, and boreal groups following rules of Nemani and Running (1996) that also used to make CLM land surface data by Peter et al. (2007; 2012) since CLM version 3

<sup>b</sup> LGG and LGBS did not outputs PFT-level fire carbon emissions, so land cover classified using its dominant vegetation type

<sup>c</sup> MC2 classifies tropical savannas and tropical deciduous woodland regions, and the latter mainly represents tropical deciduous forests

**Table 5.** Summary description of satellite-based products and historical constructions

merged from multiple sources.

Name	Method	Fire data sources	Peat burning	Start year	reference
GFED4	Bottom-up: fuel consumption,	MODIS, VIRS/ATSR	Y	1997	van der Werf et al. (2017)
GFED4s	burned area & active fire counts		Y	1997	
GFAS1.2	(GFED4&4s), FRP (GFAS1),	MODIS	Y	2001	Kaiser et al. (2012)
FINN1.5	active fire counts (FINN1.5), emis. factor	MODIS	N	2003	Wiedinmyer et al. (2011)
FEER1	Top-down: FRP, satellite AOD	MODIS, SEVIRI	Y	2003	Ichoku and Ellison (2014)
QFED2.5	constrained, emis. factor	MODIS	N	2001	Darmenov and da Silva (2015)
CMIP5	Merged decadal fire trace gas and aerosol emis.	GFED2, GICC, RETRO (model GlobFIRM used)	Y	1850	Lamarque et al. (2010)
CMIP6	Merged monthly fire carbon emis., present-day veg. dist., emis. factor	GFED4s, median of six FireMIP model sims., GCDv3 charcoal records, WMO visibility obs.	Y	1750	van Marle et al. (2017)

Acronyms: GFED4: Global Fire Emissions Dataset version 4; GFED4s: GFED4 with small fires; GFAS1.2: Global Fire Assimilation System version 1.2; FINN1.5: Fire Inventory from NCAR version 1.5; FRP: fire radiative power; FEER1: Fire emissions from the Fire Energetics and Emissions Research version1; QFED2.5: Quick Fire Emissions Dataset version 2.5; AOD: aerosol optical depth; GFED2: GFED version 2; RETRO: REanalysis of the TROpospheric chemical composition; GICC: Global Inventory for Chemistry-Climate studies; GCDv3: Global Charcoal Database version 3



**Table 6.** Global total of fire emissions from 2003 to 2008 for DGVMs in FireMIP and benchmarks. Unit: Pg (Pg=10<sup>15</sup>g)

Source	C	CO <sub>2</sub>	CO	CH <sub>4</sub>	BC	OC	PM <sub>2.5</sub>
<b>FireMIP</b>							
CLM4.5	2.1	6.5	0.36	0.018	0.0021	0.020	0.042
CTEM	3.0	8.9	0.48	0.025	0.0028	0.030	0.060
JSBACH	2.1	6.5	0.32	0.013	0.0020	0.016	0.036
JULES	2.1	6.9	0.44	0.024	0.0022	0.020	0.039
LGG	4.9	15.4	0.90	0.047	0.0050	0.048	0.097
LGS	1.7	5.6	0.26	0.011	0.0017	0.012	0.027
LGSB	2.5	7.7	0.48	0.025	0.0025	0.024	0.047
MC2	1.0	3.1	0.18	0.008	0.0011	0.012	0.025
ORCHIDEE	2.8	9.2	0.44	0.018	0.0029	0.020	0.045
<b>Benchmarks</b>							
GFED4	1.5	5.4	0.24	0.011	0.0013	0.012	0.025
GFED4s	2.2	7.3	0.35	0.015	0.0019	0.016	0.036
GFAS1.2	2.1	7.0	0.36	0.019	0.0021	0.019	0.030
FINN1.5	2.0	7.0	0.36	0.017	0.0021	0.022	0.039
FEER1	4.2	14.0	0.65	0.032	0.0042	0.032	0.054
QFED2.5	---	8.2	0.39	0.017	0.0060	0.055	0.086

**Table 7.** Temporal correlation of annual global fire PM<sub>2.5</sub> emissions between FireMIP models and satellite-based GFED4 and GFED4s (1997–2012), GFAS1.2 and QFED2.5 (2001–2012), and FINN1.5 and FEER1 (2003–2012).

DGVMs	GFED4	GFED4s	GFAS1.2	FINN1.5	FEER1	QFED2.5
CLM4.5	0.73***	0.79***	0.63**	0.62*	0.55*	0.58**
CTEM	0.51**	0.54**	0.63**	0.60*	0.52	0.68**
JSBACH	−0.18	−0.42	0.10	0.02	−0.04	0.32
JULES	0.33	0.31	0.31	0.56*	0.29	0.39
LGG	0.08	0.03	−0.15	0.01	−0.20	−0.03
LGS	0.12	0.04	−0.00	0.40	−0.01	0.08
LGSB	0.51**	0.64***	0.39	0.72**	0.56*	0.55*
ORCHIDEE	−0.13	−0.25	−0.16	0.29	−0.10	−0.10

\*, \*\*, and \*\*\* : Pearson correlation passed the Student’s t-test at the 0.1, 0.05, and 0.01 significance level, respectively.

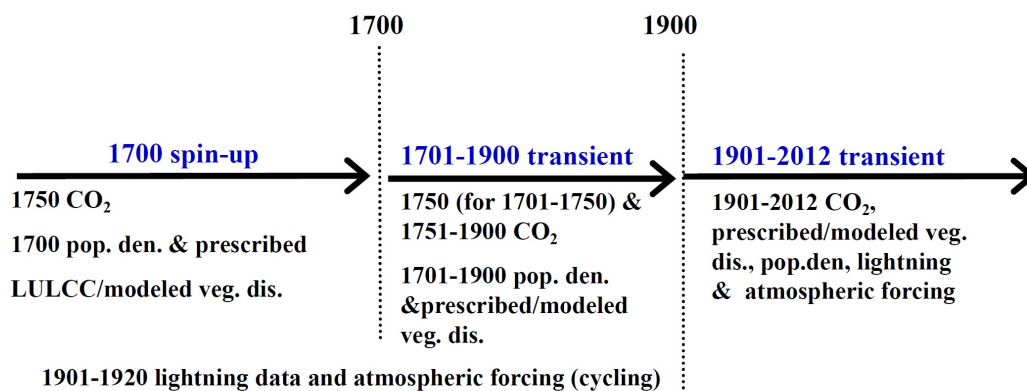


**Figure 1.** FireMIP experiment design. Note that CTEM and MC2 start at 1861 and 1901 and spin-up using 1861 and 1901 CO<sub>2</sub>, population density, and prescribed / modeled vegetation distribution, respectively.

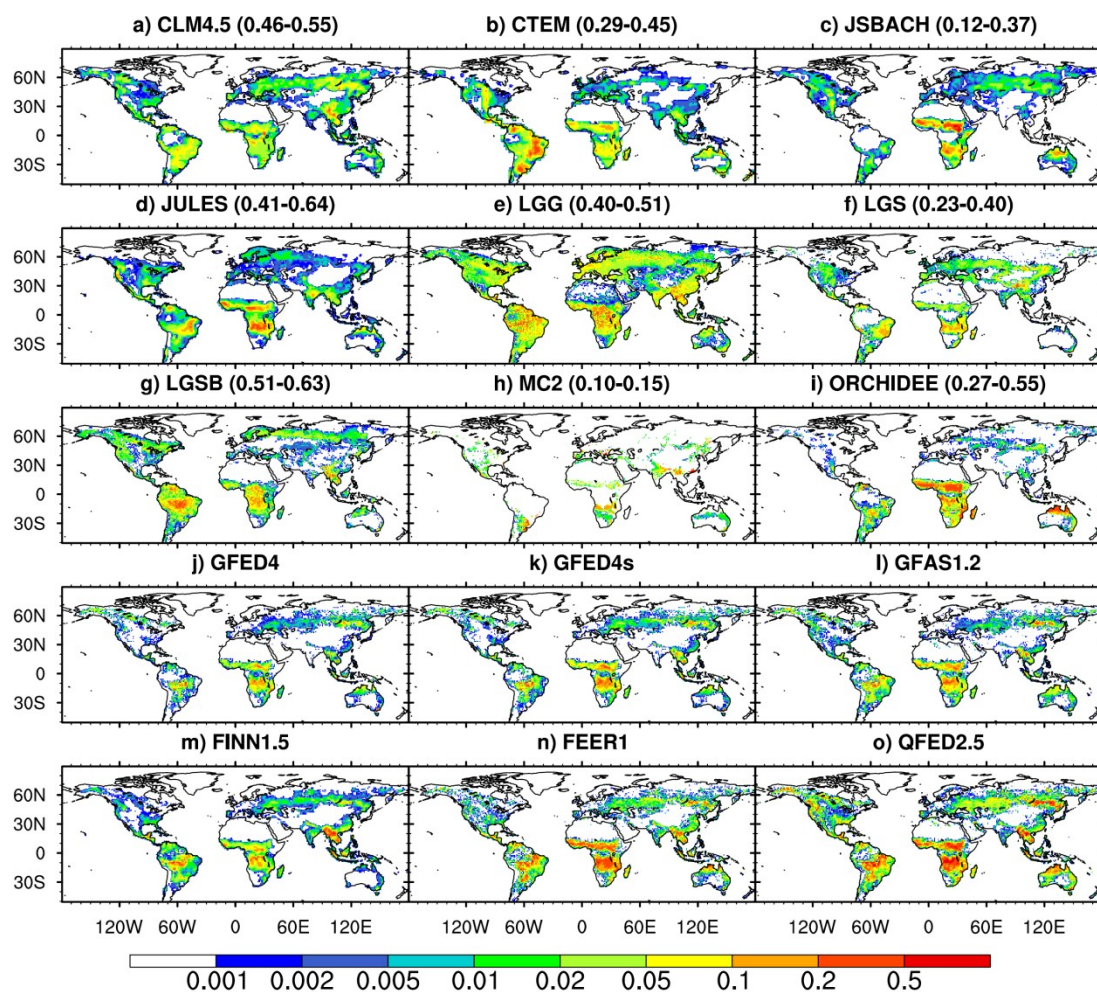


**Figure 2.** Spatial distribution of annual fire black carbon (BC) emissions ( $\text{g BC m}^{-2} \text{yr}^{-1}$ ) averaged over 2003–2008. The range of global spatial correlation between DGVMs and satellite-based products is also given in brackets.

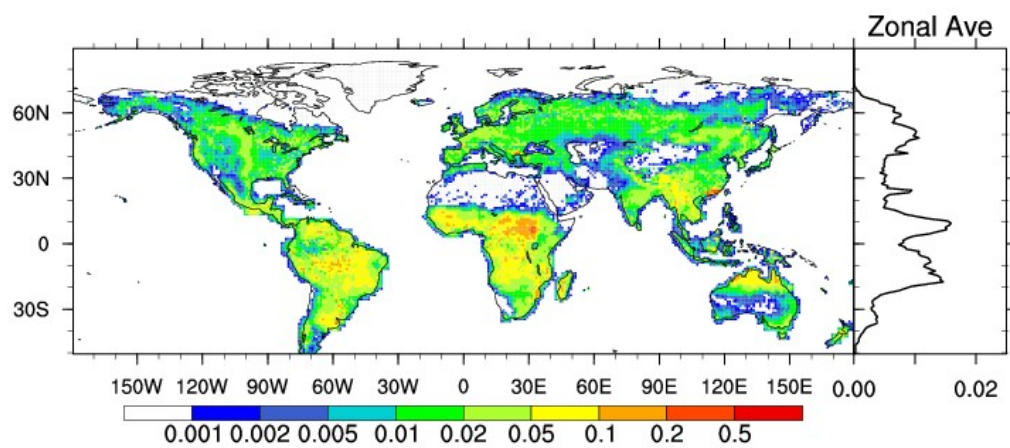


**Figure 3.** Inter-model standard deviation of 2003–2008 averaged fire BC emissions ( $\text{g BC m}^{-2} \text{yr}^{-1}$ ) in FireMIP models and the zonal average.

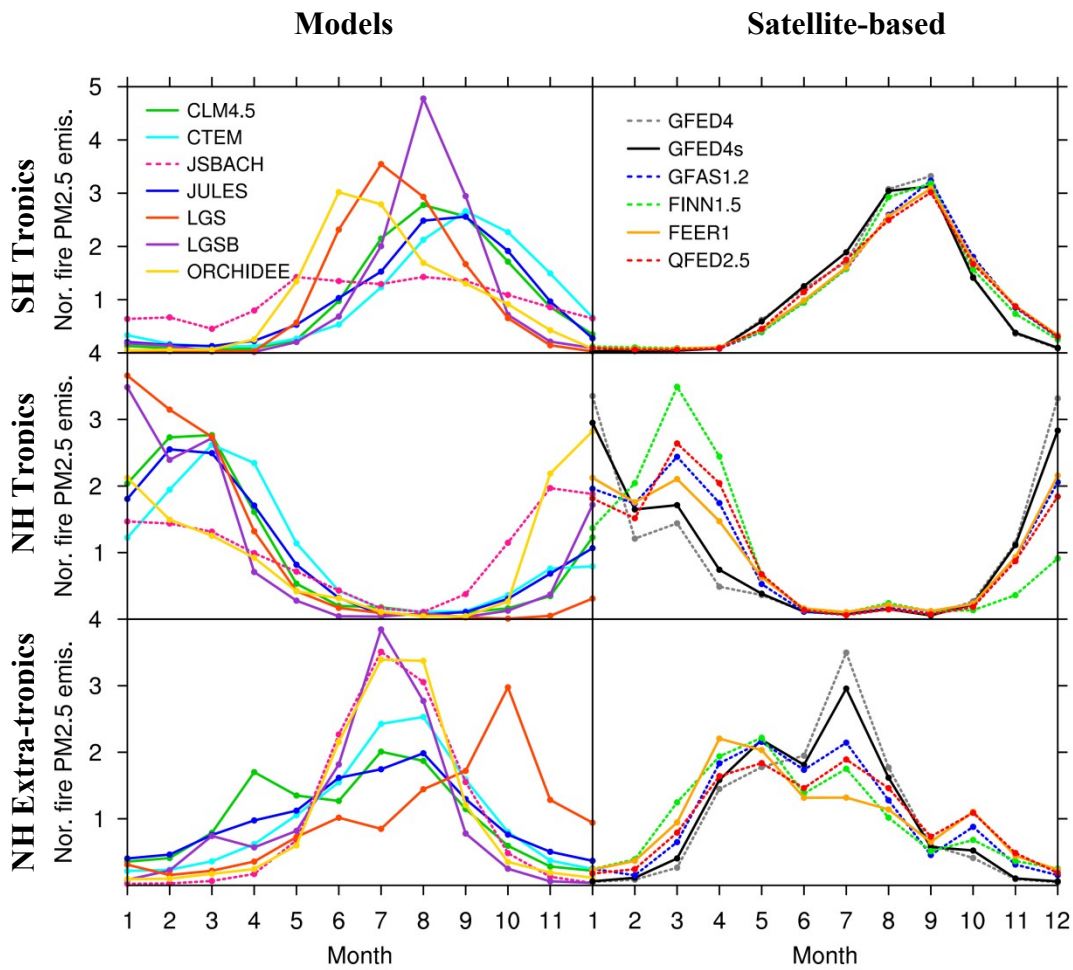


**Figure 4.** Seasonal cycle of fire  $PM_{2.5}$  emissions normalized by the mean from FireMIP models and satellite-based products averaged over 2003–2008 in the Southern Hemisphere (SH) tropics ( $0\text{--}23.5^\circ\text{S}$ ), Northern Hemisphere (NH) tropics ( $0\text{--}23.5^\circ\text{N}$ ), and NH extra-tropics ( $23.5\text{--}90^\circ\text{N}$ ). Fire emissions from LPJ-GUESS-GlobFIRM and MC2 are updated annually and thus are not included here.

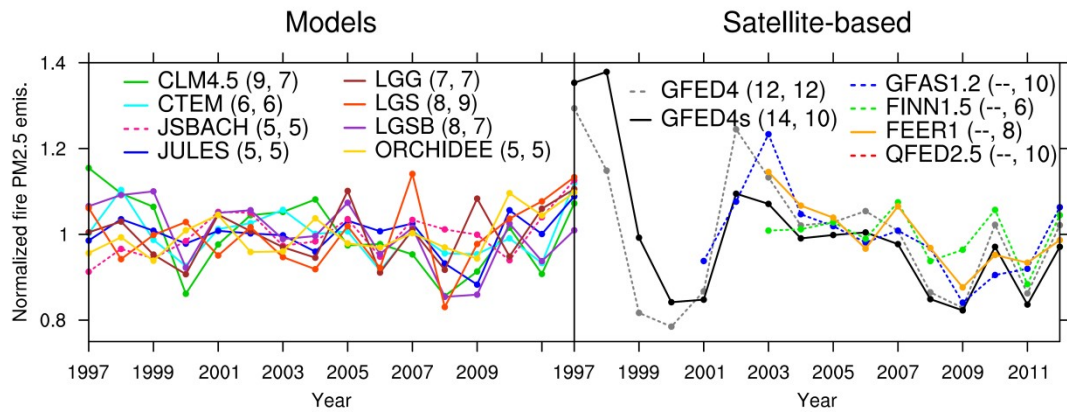


**Figure 5.** Temporal change of annual global fire  $PM_{2.5}$  emissions normalized by the mean from FireMIP models and satellite-based products. The numbers in the brackets are coefficient of variation (CV, the standard deviation divided by the mean, unit: %) for 1997–2012 and 2003–2012, respectively.

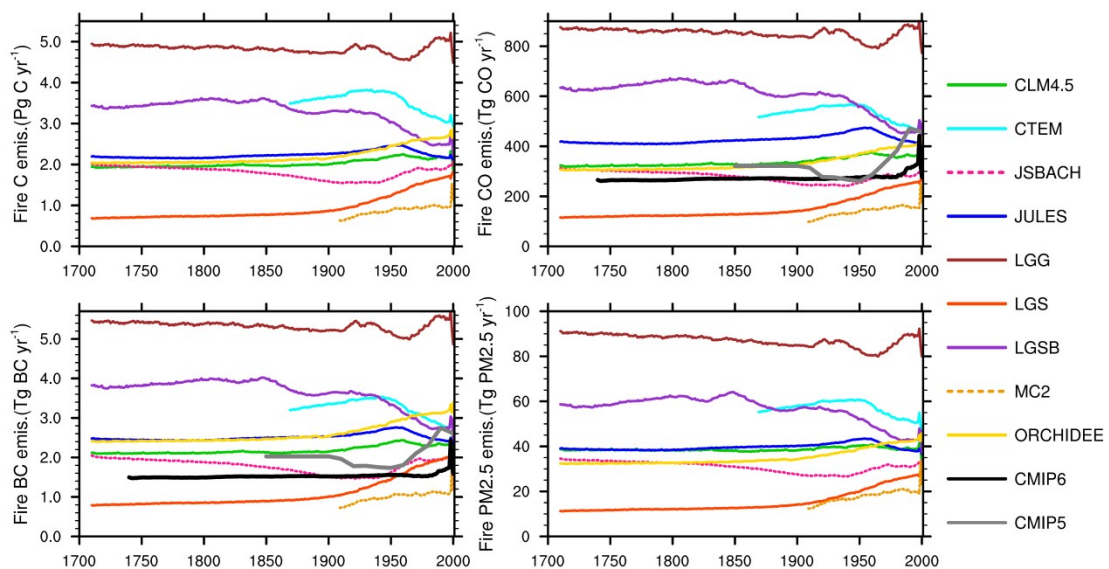


**Figure 6.** Long-term temporal change of fire emissions from DGVMs in FireMIP and CMIPs forcing. A 21-year running mean is used.

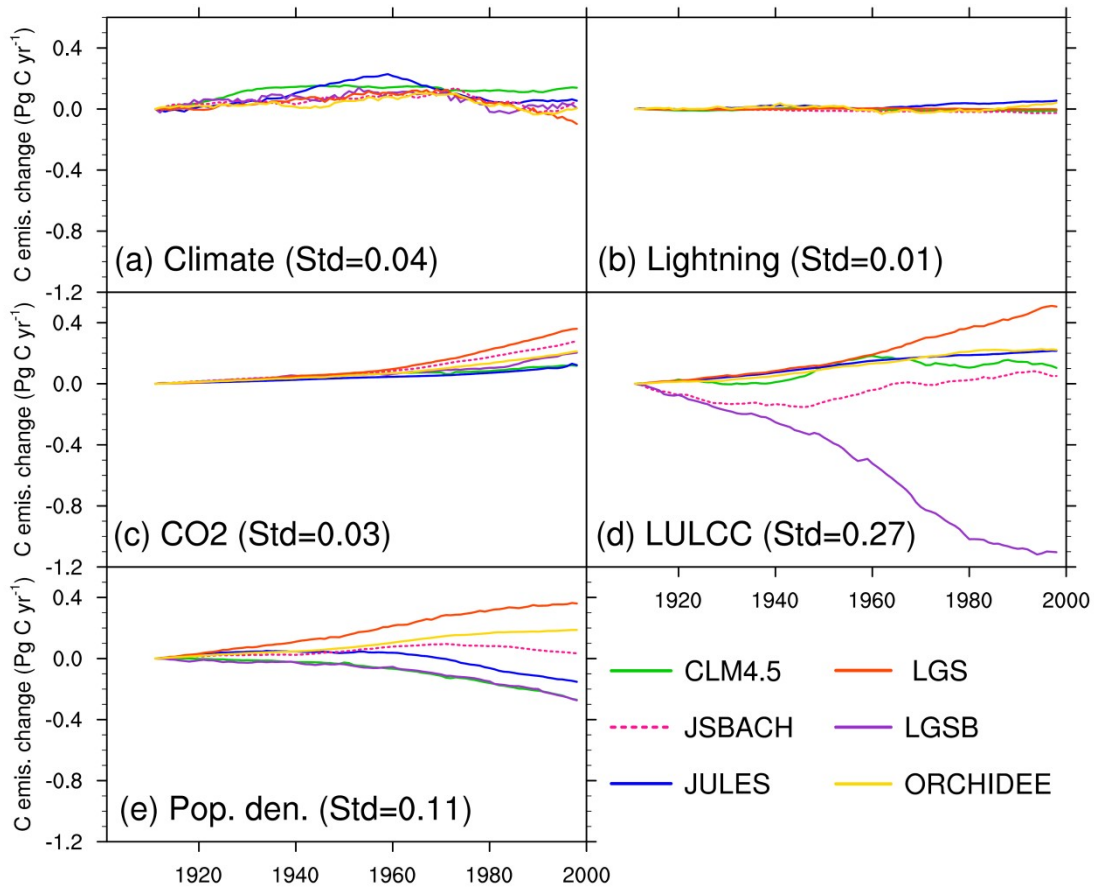


**Figure 7.** Change in global annual fire carbon emissions (Pg C yr<sup>-1</sup>) in the 20th century due to changes in (a) climate, (b) lightning frequency, (c) atmospheric CO<sub>2</sub> concentration, (d) land use and land cover change (LULCC), and (e) population density (control run – sensitivity run). A 21-year running mean is used. The standard deviation (Std) of multi-model simulated long-term changes averaged over the 20th century is also given in the bracket. Control run is normal transient run, and five sensitivity runs are similar to the control run but without change in climate, lightning frequency, atmospheric CO<sub>2</sub> concentration, land cover, and population density, respectively. The 20th century changes of driving forces used in FireMIP are characterized by an increase in the global land temperature, precipitation, lightning

frequency, atmospheric CO<sub>2</sub> concentration, and population density, expansion of croplands and pastures, and a decrease in the global forest area.

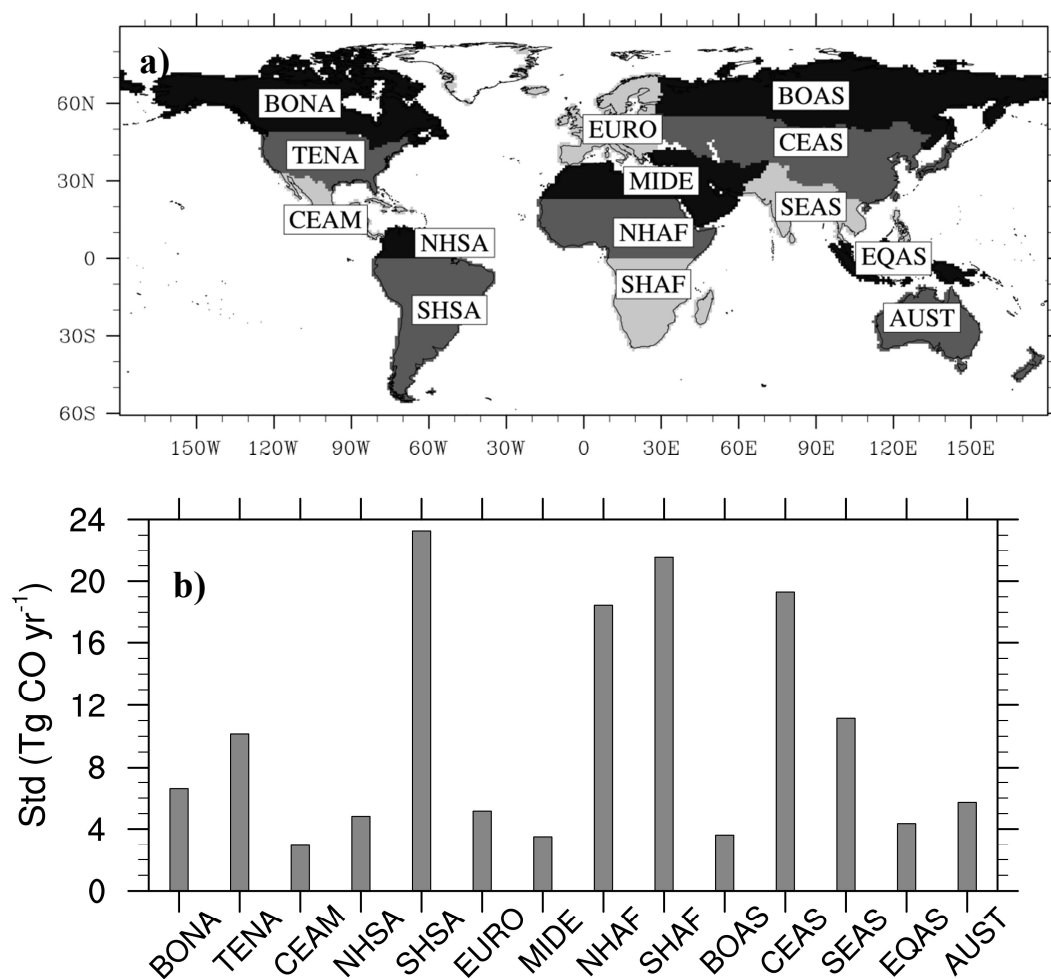


**Figure 8.** a) GFED region definition (<http://www.globalfiredata.org/data.html>), and b) inter-model discrepancy (quantified using inter-model standard deviation) in long-term changes (a 21-year running mean is used, relative to present-day) of simulated regional fire CO emissions (Tg CO yr<sup>-1</sup>) averaged over 1700–2012 (calculate long-term changes relative to present-day for each FireMIP model first, then the inter-model standard deviation, and lastly the time-average). Acronyms are



BONA: Boreal North America; TENA: Temperate North America; CEAM: Central America; NHSA: Northern Hem. South America; SHSA: Southern Hem. South America; EURO: Europe; MIDE: Middle East; NHAf: Northern Hem. Africa; SHAF: Southern Hem. Africa; BOAS: Boreal Asia; CEAS: Central Asia; SEAS: Southeast Asia; EQAS: Equatorial Asia; AUST: Australia.

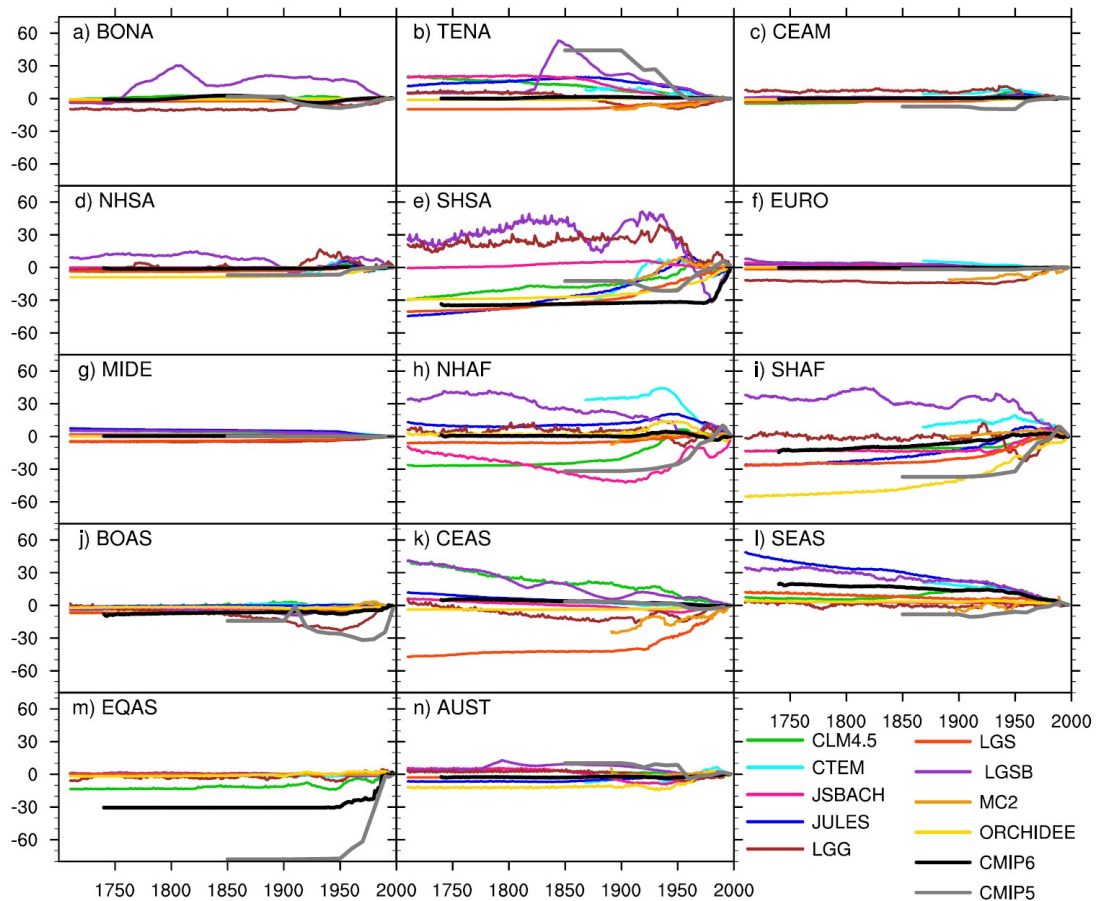


**Figure 9.** Long-term changes of annual regional fire CO emissions ( $\text{Tg CO yr}^{-1}$ ) from FireMIP models and CMIPs. A 21-year running mean is used.